



# FINAL PUBLISHABLE REPORT

Grant Agreement number            15SIB09  
 Project short name                    3DNano  
 Project full title                      Traceable three-dimensional nanometrology

Project start date and duration:		01 October 2016, 36 months
Coordinator: Virpi Korpelainen, Dr., VTT		Tel: +358 50 410 5504            E-mail: <a href="mailto:virpi.korpelainen@vtt.fi">virpi.korpelainen@vtt.fi</a>
Project website address: <a href="https://www.ptb.de/emrp/15sib09-home.html">https://www.ptb.de/emrp/15sib09-home.html</a>		
Internal Funded Partners:	External Funded Partners:	Unfunded Partners:
1 VTT, Finland	8 FAU, Germany	11 INRIM, Italy
2 CMI, Czech Republic	9 NCSR Demokritos, Greece	12 METAS, Switzerland
3 DFM, Denmark	10 TNO, Netherlands	
4 NPL, United Kingdom		
5 PTB, Germany		
6 SMD, Belgium		
7 VSL, Netherlands		
RMG: -		

**Report Status: PU Public**

*This publication reflects only the author's view and the Commission is not responsible for any use that may be made of the information it contains.*

**EMPIR**    
 The EMPIR initiative is co-funded by the European Union's Horizon 2020 research and innovation programme and the EMPIR Participating States

Final Publishable Report

## TABLE OF CONTENTS

1	Overview .....	3
2	Need .....	3
3	Objectives .....	3
4	Results .....	4
4.1	Reducing uncertainty & noise level and improving scanning speed & range .....	4
4.1.1	Reducing the 3D nanomeasurement uncertainty to less than 1 nm using a bottom up approach...	4
4.1.2	Reduction of noise level of MAFMs to 0.1 nm (rms) using top-down approach .....	8
4.1.3	Raising the scanning speed up to 1 mm/s and extending the scanning range up to 25 mm .....	11
4.1.4	Summary of key research outputs .....	13
4.2	Development of reference materials for 3D nanometrology tools .....	14
4.2.1	Design and production of reference materials .....	14
4.2.2	Characterisation of reference materials .....	17
4.2.3	Summary of key research outputs and conclusions .....	24
4.3	Widening the understanding of probe-sample interactions in AFM and SEM measurements	25
4.3.1	Probe-sample interaction force .....	25
4.3.2	Data analysis of AFM data .....	26
4.3.2	Role of humidity in SPM measurements .....	27
4.3.3	Summary of key research outputs and conclusions .....	30
4.4	Development of a hybrid metrology for merging measurement results .....	30
4.4.1	Software for data fusion .....	30
4.4.2	Hybrid metrology of AFM and TEM for bottom-up approach .....	32
4.4.3	Hybrid metrology with optical scatterometry and MAFM .....	32
4.4.4	Summary of key research outputs and conclusions .....	33
5	Impact .....	33
6	List of publications .....	35
7	Contact details .....	35

## 1 Overview

The overall goal of this project was to meet future requirements for traceable 3-dimensional (3D) metrology at the nanometre level with measurement uncertainties below 1 nm. To achieve this goal the project set up to establish new routes for traceability, further developed existing instruments and validated 3D measurement procedures. Moreover, the project developed new calibration artefacts that can be used in industry as traceable reference standards to enable valid comparison of fabrication and measurement results, and establish a robust basis for design of objects with traceable nanoscale dimensions and tolerances.

## 2 Need

Nanotechnology is increasingly used in different sectors e.g. health, medicine, nanophotonics and nanoelectronics. Nanostructured materials and the market for final products incorporating nanotechnology is estimated to have increased ten-fold during the current decade. The progressive miniaturisation of advanced nanomanufacturing techniques and the extensive use of complex nano-objects of different shapes (rod, star, donut shape, etc.) has driven the need for improved accuracy in 3D nanometrology.

High-accuracy measurements are needed in R&D and quality control, as many health and environmental effects of nano-objects and nanoparticles are dependent on the size and shape of structures. From a regulatory perspective, traceability is demanded for the measurement techniques; if measurements are not traceable, they have little value from a judicial point of view. At the start of the project, there was insufficient traceability to the SI metre for true 3D nano measurements, because the level of uncertainty in measurements (5 nm) did not meet the requirements of industry or scientific research.

Scanning Probe Microscopes (SPMs) available in national metrology institutes (NMIs) have low uncertainties, are traceable to the SI-metre and significantly outperform commercial SPMs in accuracy. However, there was a large gap between these SPMs and real practical 3D measurements. To bridge the gap, instruments with lower noise, higher speed and larger range and new types of reference materials needed to be developed. Hybrid metrology is a promising way to measure complex nanostructures but it lacked data fusion software to make it a practical method.

Understanding probe-sample interactions is a key for improving uncertainty in measurements of 3D nano-structures. Prior to the start of the project, tip probe-sample interaction studies were limited to measurements of nearly flat surfaces, only. Without proper calibration and understanding of the probe-sample effects, traceability is rarely established and errors in simple measurements can be up to 30 % even with high-resolution instruments.

## 3 Objectives

The overall objective of this project was the realisation of traceable calibration services for three-dimensional nanometrology with an uncertainty less than 1 nm. The technical objectives of this project were to:

1. Reduce the 3D nanomeasurement uncertainty, by means of a bottom up approach, to less than 1 nm for nanodimensional measurands (including line width, height, pitch, and edge/width roughness) on engineered nanostructures and nanoparticles. In addition, to reduce the noise level of metrological AFMs (MAFMs) to 0.1 nm (rms) using a top-down approach, to raise the scanning speed up to 1 mm/s, and to extend the scanning range up to 25 mm by further developing the state-of-the-art optical and x-ray interferometry (XRI).
2. Develop reference materials for 3D nanometrology tools including AFM and SEM. In particular, to realise test structures for characterising the tip geometry in AFMs

3. Widen the understanding of probe-sample interactions in AFM and SEM measurements for reducing the measurement uncertainty. In particular, to study the tip-sample interaction force of AFM line width and nanoparticle measurements; to model the image formation of SEM; and to investigate the influence of humidity on AFM measurements.
4. Develop a hybrid metrology for merging measurement results from either different tools (e.g. AFM, SEM, TEM, Mueller polarimetry and optical scatterometry) or different channels of a single tool.
5. Facilitate the take up of the technology and measurement infrastructure developed by the project by the measurement supply chain (accredited laboratories, instrument manufacturers) and end users (semiconductor industry, precision engineering, optical industry and nanoparticle researchers).

## 4 Results

### 4.1 Reducing uncertainty & noise level and improving scanning speed & range

At the start of the project, traceability to the SI metre for true 3D nanomeasurements was insufficient, and the existing uncertainty level (5 nm) did not meet the requirements of industry and scientific research. Moreover, the measurement capabilities of metrological Atomic Force Microscopy (AFMs) needed to be improved to make measurements more rapid and to allow larger measurement areas and better accuracy. For instance, the interferometers used in those devices usually have a noise level above 2 nm (peak to peak), which greatly limits their measurement performance, and most Metrological Atomic Force Microscopy (MAFMs) had a limited measurement range (typically tens of micrometres) and speed (typically tens of micrometres per second).

In order to reduce 3D measurement uncertainty to below 1 nm a new bottom-up approach using the cross-section of Transmission Electron Microscopy (TEM) structures with atomic resolution was developed. In this way, the critical dimension (CD) can be directly linked to the atomic spacing in the crystal lattice, which can be traceably calibrated using a combined optical and X-ray interferometry. Additionally, tools and measurement procedures were optimised for true 3D measurands, and AFM tips were characterised and developed for metrology at the nanometre range. Furthermore, improved displacement measurement sensors were applied in the MAFMs, in order to lower noise to 0.1 nm root mean square (rms), to reduce nonlinearity errors and to increase the range of the positioning stages to 25 mm. To address the current speed limitations for AFM metrology and progress beyond the state of the art, two approaches were followed: i) the development of high speed AFM heads that are suitable for NMI based instrumentation and video rate AFMs (scanning speed over 1 mm/s), and ii) the application of metrology to video rate AFMs that surpass the speed of current speed of MAFMs.

#### 4.1.1 Reducing the 3D nanomeasurement uncertainty to less than 1 nm using a bottom up approach

The project developed and realised a new bottom-up traceability approach in which the 3D dimension of complex nanostructures is determined by using the lattice of crystal silicon as an internal ruler, where the lattice constant was calibrated accurately and traceably by x-ray interferometers (XRI). High-resolution transmission electron microscope (HR-TEM) was applied to measure sample lamellas with a true atomic resolution, where the lamellas are prepared from the pre-defined sample structures using a focused ion beam (FIB) facility. Hybrid metrology method was used to overcome the problem that the sample preparation by the FIB technique is destructive. A detailed measurement strategy was planned; software developed and measurement experiments carried out. The final measurement uncertainty budget indicates that the critical dimension of structures can be determined at a combined standard measurement uncertainty of 0.81 nm.

#### Concept

With the development of modern spherical aberration correction technique, currently the (scanning) transmission electron microscopes (S)TEMs are capable of microscopic imaging with a spatial resolution down to 0.05 nm, i.e. true atomic resolution. Such outstanding imaging power offers new solutions for nanometrology. As illustrated in Figure 1, if the atoms in the nanostructures are resolvable, its dimensional parameters (shown as the line width) can be determined by using the atom spacing as an internal "ruler".

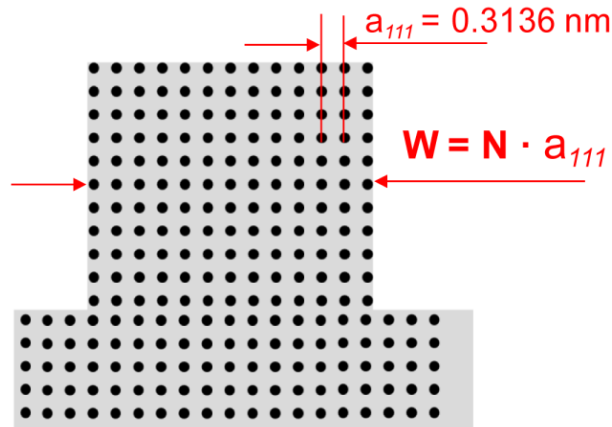


Figure 1. Basic idea for the determination of feature width using crystal lattice constant as an internal “ruler”.

### Realisation

There are several important aspects in the realisation of the bottom up traceability route for CD metrology: preparation of TEM lamella, TEM measurements and the assignment of feature edges in high resolution (S)TEM images.

High quality TEM lamella is an important pre-requisite for obtaining TEM images with true atomic resolution. Today, more and more TEM lamellas are prepared by means of focus ion beam (FIB) tools. However, the ion-beam-induced *amorphization* will lead to the alteration of the structure under measured, and finally resulting in measurement bias. To avoid such problem, the structure needs to be well protected by suitable coating layers, which were chosen as carbon and platinum layers in our study, before being FIB processed. A set of typical TEM lamella processes are illustrated in Figure 2.

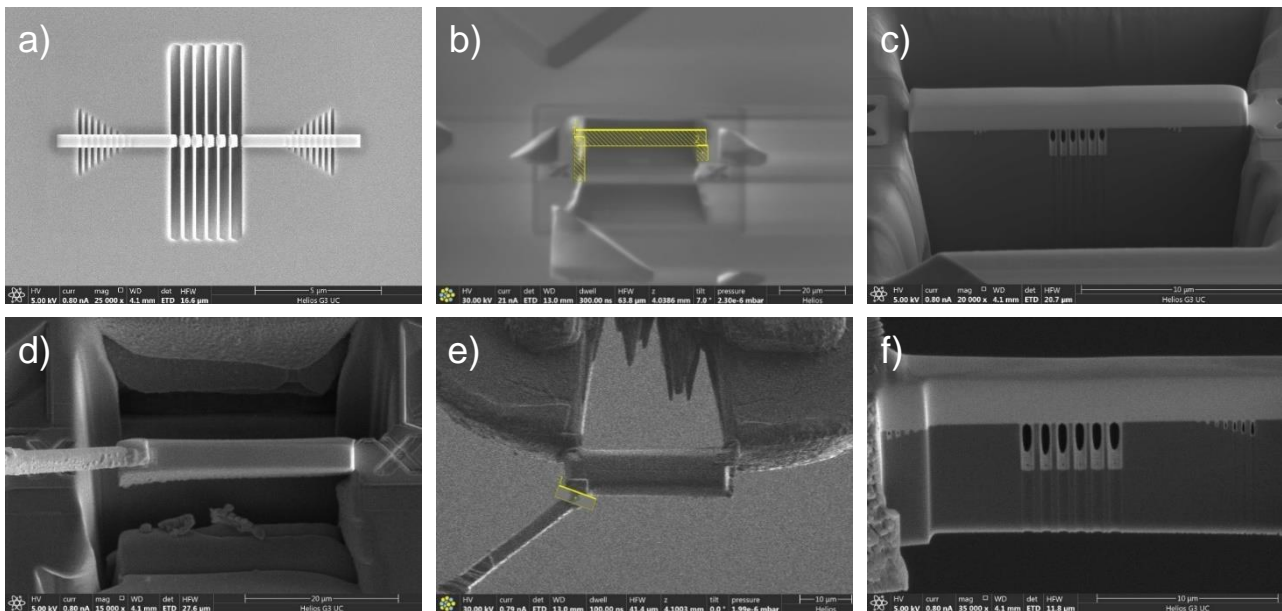


Figure 2. Procedures of TEM lamella preparation, shown as (a) Protect layers deposition: first carbon and then platinum; (b) FIB milling for preparing the lamella; (c) FIB milling finished at both sides; (d) Wire attached to the lamella for lifting out the prepared lamella; (e) Attachment of the lifted out lamella to a sample holder of TEM named as “finger”; (f) fine FIB milling/polishing of the lamella to the desired thickness of about 50 nm.

After the lamella is prepared, it can be inserted into a TEM tool for measurements. After fine adjusting of measuring parameters, such as the beam and field aberration correction, the alignment of the sample and the

adjustment of the focus point, fine (Scanning) Transmission Electron Microscopy ((S)TEM) image can be obtained as demonstrated in Figure 3. As shown in the figure, the atom spacing between the crystal planes {1 1 1},  $a_{111}$ , can be used as an internal “ruler” for measurements.

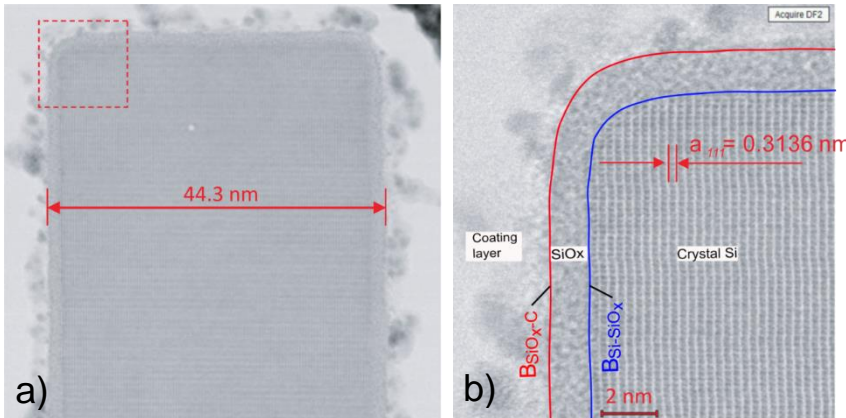


Figure 3. Width of a crystal silicon line feature determined by the bottom-up approach, shown as (a) the measured STEM image of the line feature; and (b) the zoom-in view of the image at the marked box in (a), where the crystal plane is clearly visible for being applied as an internal ruler.

To apply the bottom up approach in practice, it remains as a challenging issue to accurately assign the feature edges in high resolution (S)TEM images. Our study suggested that the feature edge should be better defined as the half intensity position for STEM images. The definition is analogue to the edge assignment issue in conventional optical microscopic images measured with an incoherent light source. Physically it stands for the edge location where the material occupation is about 1:1. This edge definition is adopted in this study, and the width of the line feature is determined as  $(44.3 \pm 0.3)$  nm for the example shown in Figure 4. This result is also traceable to the SI unit of metre via an unbroken calibration chain. It is worth mentioning that the uncertainty is driven much more by determining the edge position of the SiOx-C boundary than the lattice spacing.

Dissemination

Another remaining problem in applying the bottom up traceability route mentioned above is the dissemination issue. As the sample needs to be destructively TEM measured, it is no more available for further applications. To solve this problem, a strategy for non-destructive calibration is suggested in Figure 4. The strategy consists of three steps. In the first step, two groups of specimens are selected, one as the reference structures and the other as the TEM target structures. The two groups of specimens are measured by the CD-AFM using the same flared tip under the same measurement conditions. Their results are registered. In the second step, the TEM target structures are measured destructively and their dimension can be evaluated. In the third step, the (effective) tip geometry can be evaluated based on the TEM reference values. With the known (effective) tip geometry, the dimension of the reference structures can be calculated, too. Although the reference structures were not measured by TEM, they can be well applied for reference metrology.

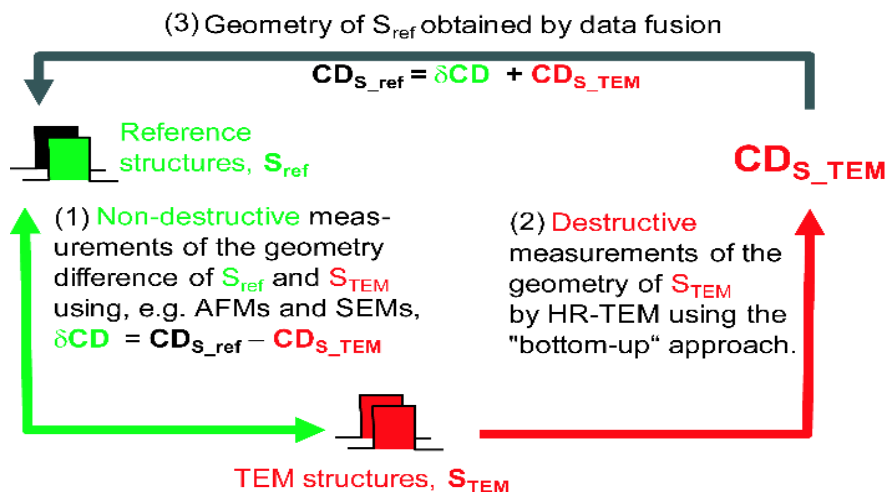


Figure 4. Strategy for disseminating the bottom-up route calibration results for non-destructive calibrations.

### Application

The developed bottom up traceability route can be applied to calibrate e.g. probe geometry, test or benchmark CD tools, perform comparison measurements between different methods/tools as well as verify theoretical modelling with experimental results. The application of the line width standard (a sample type IVPS-100-PTB) calibrated using the bottom up traceability route for CD-AFM tip characterisation is given in Figure 5 as an example. The IVPS-100-PTB sample is measured by a new CDR120-EBD tip, which has a nominal tip width of 120 nm. The obtained apparent CD-AFM values (i.e. the CD values without tip correction) are plotted as the y coordinates. After the CD-AFM measurements are performed, the sample is destructively prepared and TEM measured. The obtained CD values of five line features by TEM are plotted as the x coordinates.

Fitting the obtained five data points to a linear function  $y = kx + b$ , we get:  $y = 0.9988x + 128.32$  nm

Here the parameter  $k = 0.9988$  stands for the scaling factor of our CD-AFM. It coincides well with the theoretical value 1, since the CD-AFM was calibrated to our metrological AFM in advance. The parameter  $b = 128.32$  nm is the calibrated effective width of the applied tip.

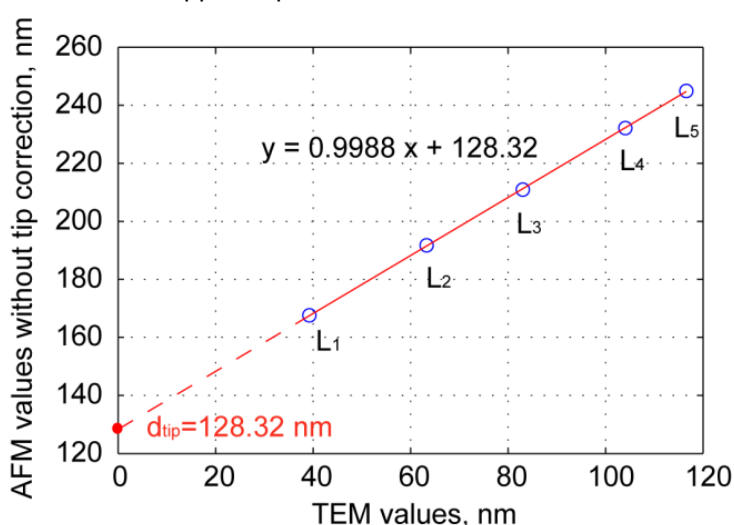


Figure 5. Calibration of the effective AFM tip width using the IVPS100-PTB standard. Five data points marked by circles indicate five pairs of TEM results and AFM results (raw data without tip correction) obtained on five line features, respectively. The red line is the least-square-fitted linear curve of the data points. The y-coordinate of the fitted curve at  $x=0$  indicates the effective width of the applied AFM tip.

### Bottom up traceability through x-ray interferometry

During the lifetime of 3D Nano PTB and NPL were working on the development of a separated crystal x-ray interferometer in combination with an atomic force microscope for long range calibration of one dimensional gratings. Bringing the x-ray interferometer into operation proved more challenging than was expected. This was due to the requirements for positioning the two components of the x-ray interferometer and the need to design an additional goniometer for angular alignment rather than relying on commercial goniometers as was originally planned. Although these issues were addressed, a solution was found too late to be implemented in the combined x-ray interferometer AFM experiment.

However, in parallel during 2018 both PTB and NPL contributed to the tasks allocated to the Consultative Committee's working Group for Nanometrology to detail a guide for realization of length traceability via the bottom up route of x-ray interferometry. The report was based on previous work together with an estimate of uncertainties associated with a separated crystal x-ray interferometer as designed for 3D nano. Measurements made with a monolithic x-ray interferometer and separated crystal x-ray interferometers using other set ups show that the target uncertainty of  $<0.1$  nm is achievable.

Results from the bottom up approach and the x-ray interferometry work performed within this project contributed to the realisation of the lattice parameter of silicon as a secondary length standard in the revised *Mise en Pratique* for the metre (<https://www.bipm.org/utis/en/pdf/si-mep/SI-App2-metre.pdf>) and to its Guidance document CCL-GD-MeP-1: "Realization of the SI metre using silicon lattice parameter and x-ray

interferometry for nanometre and sub-nanometre scale applications in dimensional nanometrology” (<https://www.bipm.org/utis/common/pdf/CC/CCL/CCL-GD-MeP-1.pdf>).

The traceability chain of the bottom-up approach is summarised in Figure 6. Nanostructures are measured using HR-TEM with true atomic resolution, thus their geometry can be related to the lattice constant of the crystal, which is calibrated to standard optical wavelength using, e.g. a combined optical and x-ray interferometer. The optical wavelength is calibrated to the SI unit metre e.g. via an optical frequency comb.

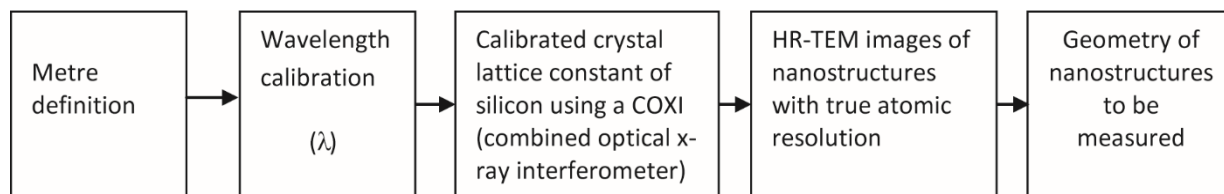


Figure 6. Traceability chain of nanoscale dimensional metrology with bottom-up approach.

#### 4.1.2 Reduction of noise level of MAFMs to 0.1 nm (rms) using top-down approach

Metrological AFMs use optical interferometers to measure the relative displacement between the AFM tip and sample and offer the advantage of direct traceability for dimensional measurements. However, the optical interferometers are very sensitive to the changes of environmental parameters such as air pressure, temperature and humidity, as well as the additional influences of ground and acoustic vibrations. Consequently, in MAFMs its noise is typically at a level of above 0.6 nm (rms). This limits the application capabilities of MAFMs, for instance for reference metrology of ultra-smooth surfaces, and is becoming one of the major limiting factors of the MAFMs. In this project, various measures have been studied and undertaken to reduce the noise level of MAFMs. For instance, for the metrological large range AFM available at PTB, some key components such as its interferometers and the angle sensors have been upgraded for easier adjustment, better thermal behaviour and better stability. The geometry of the corner mirror has been improved to fix samples so that the stress introduced into the optical component due to the sample fixing is greatly minimised. A new motorised spring mechanism has been installed for the weight compensation of the motion stage, thus reducing the heat generation for better temperature stabilisation. In addition, an improved instrument chamber for better thermal and acoustic insulation and an improved vibration damping stage are applied. With these improvements, the noise level of the metrology tool has been reduced significantly, for instance, the positioning noise along the z-axis has been improved from  $1 \sigma = 0.52 \text{ nm}$  to  $1 \sigma = 0.13 \text{ nm}$ , both measured at the sampling frequency of 6.25 kHz.

After installation of a new scanning stage into NPL's metrological AFM, the noise levels measured in the x, y and z axes are 0.25 nm, 0.55 nm and 0.31 nm. A further reduction is possible with more averaging of collected data to achieve the target of 0.1 nm rms. Noise levels in NPLs' high speed metrological AFM are between 0.1 nm and 0.4 nm depending on the mode of operation and the density of data points collected. It should be realised, that this is the first time 3 D metrology has been brought to high speed AFMs that are used for non-NMI applications.

FAU undertook various efforts to reduce the noise level of their nanomeasuring machine NMM-1, which is used for the long range AFM:

- NMM-1 new positioned on heavy granite table standing on pendulum isolators to reduce vertical and especially lateral vibrations

- a new table top damping system to eliminate vertical vibrations
- repair of two frequency-stabilized lasers (replacement of power supply units), verification of all three frequency-stabilized lasers with a frequency comb and GPS system at the University of Technology Ilmenau (now traceable to frequency and time standard)
- elimination of signal processing problems of the autocollimators for the angular control of the NMM-1 positioning stage
- a new cover for acoustic shielding, thermal isolation and temperature control

With the self-sensing AFM on the NMM-1, a noise level of 7 nm is reached (z-axis), which can be improved to 0.2 nm by filtering.

*Figure 7. NMM-1 new positioned on heavy granite table standing on pendulum isolators and with new cover for acoustic shielding and isolation.*



At CMI the measurement uncertainty of the metrology AFM was reduced on basis of numerical simulations of the probe-sample interaction. The probe shape related uncertainty was the dominant effect for many nanoscale dimensional measurements and with novel tools for simulation of the blind tip estimation process performance and with better measurement strategies to reduce the impact of noise on the blind tip estimated data this component was reduced.

VSL demonstrated 0.1 nm rms noise level for their 3D AFM. During the 3DNano project the system broke down and no additional measurements could be performed with this instrument.

VTT have totally redesigned its MAFM for 3D measurements in order to reduce the noise level and to achieve a larger measurement range. Furthermore, the measurement software was updated. The aim of these modifications is to reduce uncertainty in calibration of transfer standards and other demanding measurements. The MAFM was designed with a highly symmetric frame, short metrology loops, vibration isolation, thermal stability, and interferometric scales that comply with the Abbe principle.

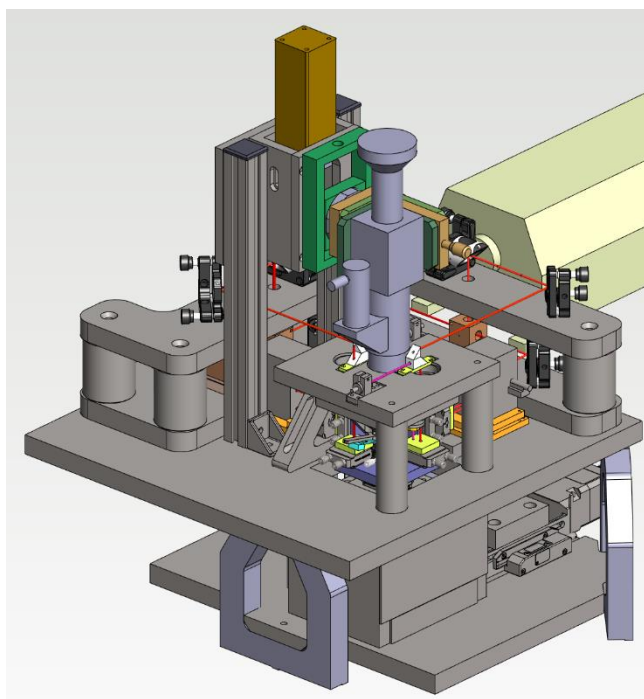


*Figure 8. The new design of VTT MIKES MAFM.*

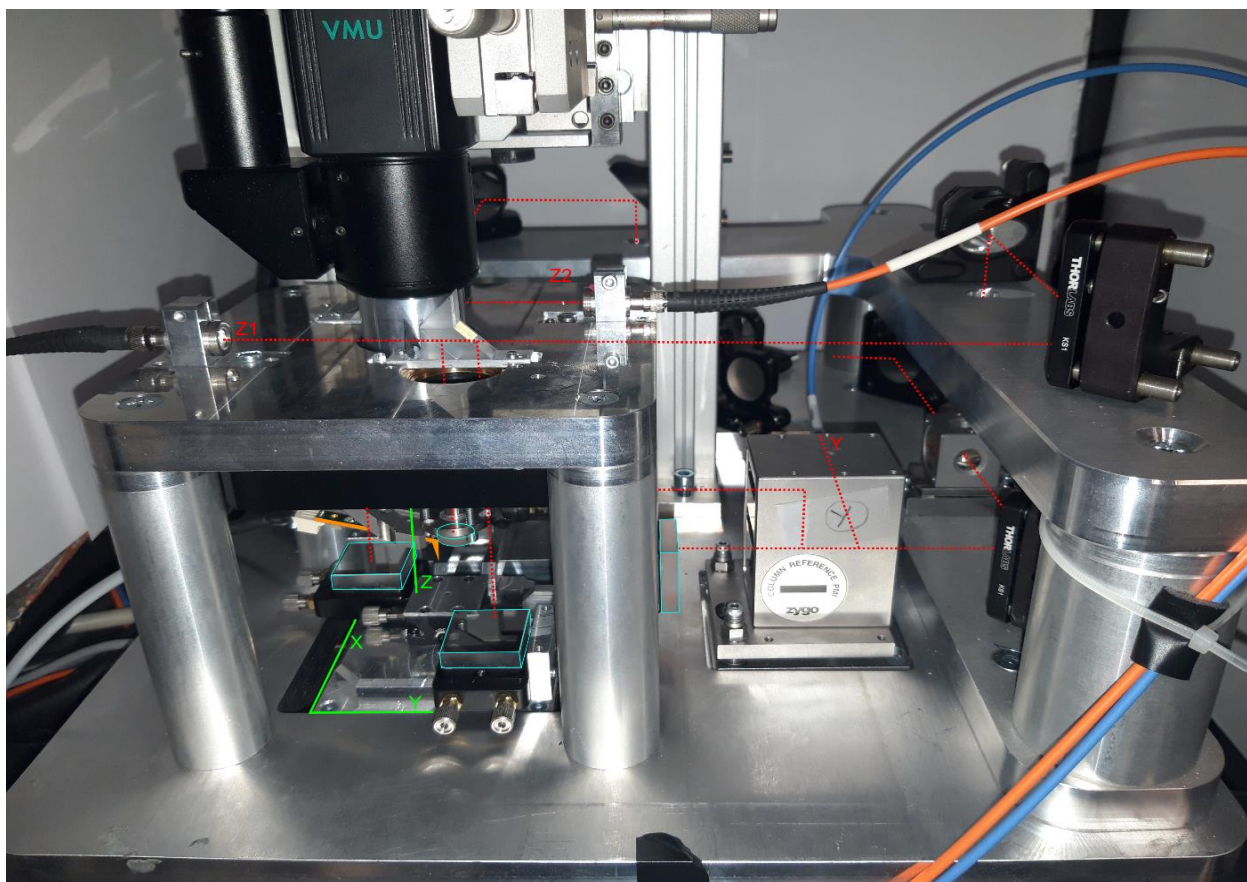


Figure 9. MIKES MAFM setup, shown with motion axes (green), mirrors (teal), and interferometric axes (red).

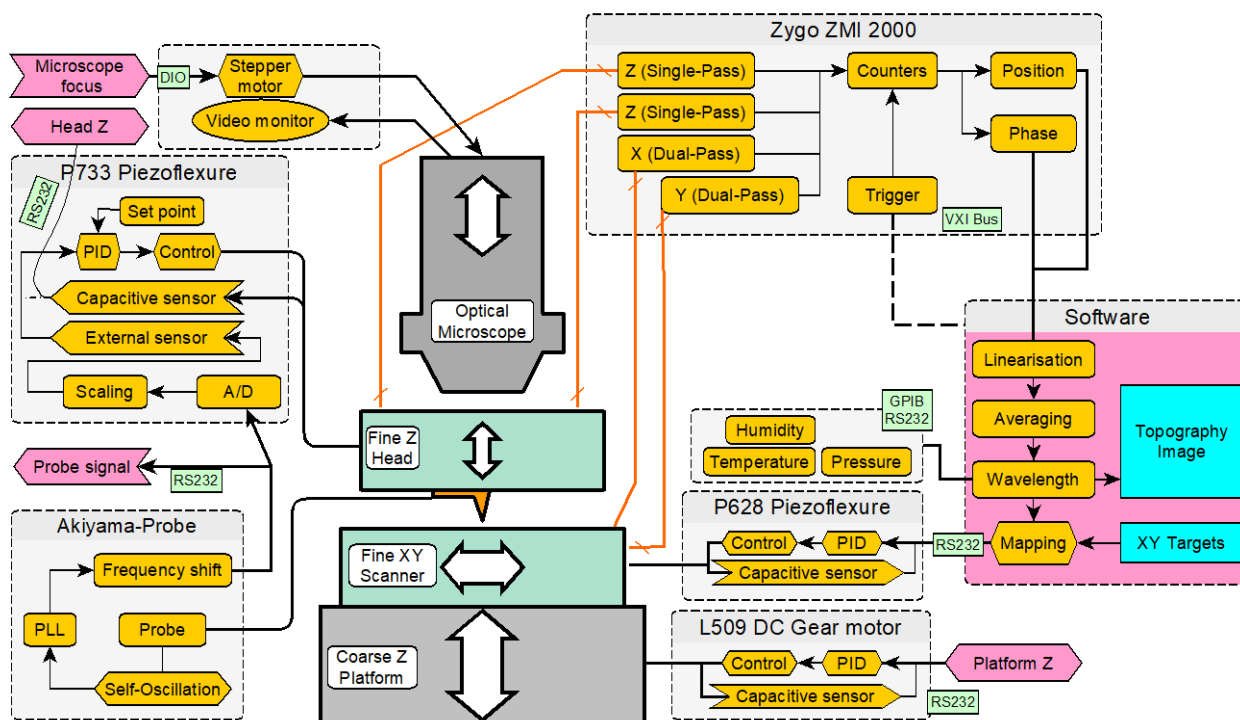


Figure 10. Core schematic of the MIKES MAFM and software interoperation.

Key components of the MAFM are its scanning system, the XYZ-interferometers, and the AFM probe (Figure 9). A maximum measurement volume of  $(950 \mu\text{m}) \times (950 \mu\text{m}) \times (115 \mu\text{m})$  is achieved using a PI-P628 piezoflexure stage for in-plane translation (XY), and a PI-P733 for vertical translation (Z). Samples are scanned in-plane while the AFM probe's oscillation is kept fixed using a feedback loop with the Z-stage. XYZ-displacement is monitored using differential heterodyne interferometers: two commercial double-pass interferometers for XY-displacement of sample, and two single-pass interferometers for Z-displacement of the AFM head. Periodic non-linearity of the interferometers is corrected by a method using an uncalibrated external sensor - in this case capacitive sensor scales of the piezoflexure stages.

In the highly stable laboratory environment, thermal expansion of the MAFM frame happens solely because of heat buildup from active components. Expansion causes instrument drift, which is counteracted by a symmetric construction and by even spreading of heat. The MAFM's aluminium frame quickly dissipates heat, counteracting non-volumetric thermal expansion. Although thermal expansion is not fully countered, the shortness of metrology loops - due to differential configuration of interferometers - mean that the effect on measurements is small. High temperature stability of the laboratory ensures that expansion of the frame due to changes in ambient conditions is small.

The MAFM is housed inside an acoustically shielded enclosure, on a vibration-isolated table. The enclosure's air humidity can be actively regulated, as humidity affects probe-sample interaction and may cause imaging errors. The MAFM also features online wavelength correction using the updated Edlén formula.

Measurement uncertainty for the MAFM is evaluated using a simple Monte Carlo method and a virtual instrument (VAFM). Having identified the distributions associated with the MAFM's - and thus the VAFM's - components, uncertainty is obtained through sampling and statistical analysis. This approach handles non-linear models without added complexity, enabling straightforward uncertainty evaluation for complicated and non-approximate system models.

Preliminary tests show that noise level of 0.2 nm can be reached in interferometric measurements of the Z direction.

#### **4.1.3. Raising the scanning speed up to 1 mm/s and extending the scanning range up to 25 mm**

Compared to other nanodimensional techniques such as optical microscopy, optical scatterometry, and scanning electron microscopy, the AFM technique has advantages of high spatial resolution, 3D and less model-dependent. In addition, it is capable of measuring in ambient, in liquid and in vacuum. These advantages make the AFM technique widely applicable for various nanometrology applications. However, the AFM technique has two major limiting factors. Firstly, as most of AFMs are based on a kind of piezo scanner. Their scan range are typically limited to tens of  $\mu\text{m}$ , which limits its application in measuring relatively large size structures or surfaces. Secondly, as a tip scanning method, till now the low measurement speed remains as a major shortcoming of the LR-AFMs. It leads not only to a low measurement throughput, but also to a significant measurement drift over the long measurement time (up to hours or even days), particularly for measurements over a large area.

To overcome this challenging issue, in this project PTB further improved our metrological large-range AFMs (Met. LR-AFMs). Compared to conventional AFMs available in industry, such Met. LR-AFM is based on ultra-precision mechanical motion stage, for instance, the so-called nanopositioning and nanomeasuring machine (NMM), or large-range flexure-hinge-stage, whose position is highly precisely measured and then servo-controlled by embedded laser interferometers as mentioned in 4.1.2.

To raise the measurement speed of Met. LR-AFM, further improvements have been undertaken in its design. For instance, the contact AFM mode is applied instead of the intermittent and non-contact modes, which offers shorter AFM response time and larger AFM sensing range. During measurements, the sample is scanned in the xy-plane solely by the NMM (such a motion usually has a constant velocity, therefore, high dynamics of the xy-scanner is not needed), meanwhile a high dynamic z-motion of the sample is realised by a combined piezo stage and the z-stage of the NMM controlled in parallel. The AFM output signal is combined with the position readouts of the piezo stage and the NMM to derive the surface topography. The combination of these readouts offers a large bandwidth of measurement signals, thus provides high speed measurement capability. Furthermore, two important means are taken to reduce the distortion in measured profiles, namely (a) the time delay of sensor signals is corrected; (b) the position sensors of the AFM and piezo stage are traceably calibrated to the z-interferometer of the NMM in situ.

With these developments, high-speed (up to 1 mm/s) and large range (up to 25 mm) metrological AFMs have been successfully realised. Verification measurements indicate that the tool can calibrate the step height standards with a stability of better than 0.8 nm (p-v), and calibrate the pitch value of a 2D grating (nominal pitch of 1000 nm) with a stability better than 0.01 nm (p-v), when the measurement speeds are increased from 10  $\mu\text{m/s}$  to 1000  $\mu\text{m/s}$  (i.e. 100x times faster).

NPL's approach was to collaborate with non-NMI developers of HS-AFM (university of Bristol) and to bring metrology to a high speed AFM. The high speed stage on the high speed AFM has a range of 4.5  $\mu\text{m}$  and is driven with sinusoidal signals of 1 kHz and 1 Hz in x and y respectively. This corresponds to an average speed in the fast axis that is higher than the target 1 mm/sec; in fact, approaching 9 mm/sec. The high speed stage is mounted on an x-y slip stick stage with a larger range (25 mm x 25 mm) and via a combination of movements an extended range of movement is possible. However, in practice, contamination of the samples examined has prevented long range scans, the largest scan achieved so far is 0.5 mm but has 2.4 billion data points.

FAU developed a compact optical AFM head (Figure 11), which includes a laser interferometer for measuring the AFM's height and simultaneously incorporates an optical tilt measurement to acquire the orientation of the cantilever (bending and torsion). This development enables future scientific investigations to increase measuring accuracy and measuring speed and to compare the different optical measuring methods.

Integrated into the NMM-1 it offers a scanning range up to 25 mm. The electronic and digital evaluation is designed to excite the cantilever in higher modes in order to increase the measuring speed.

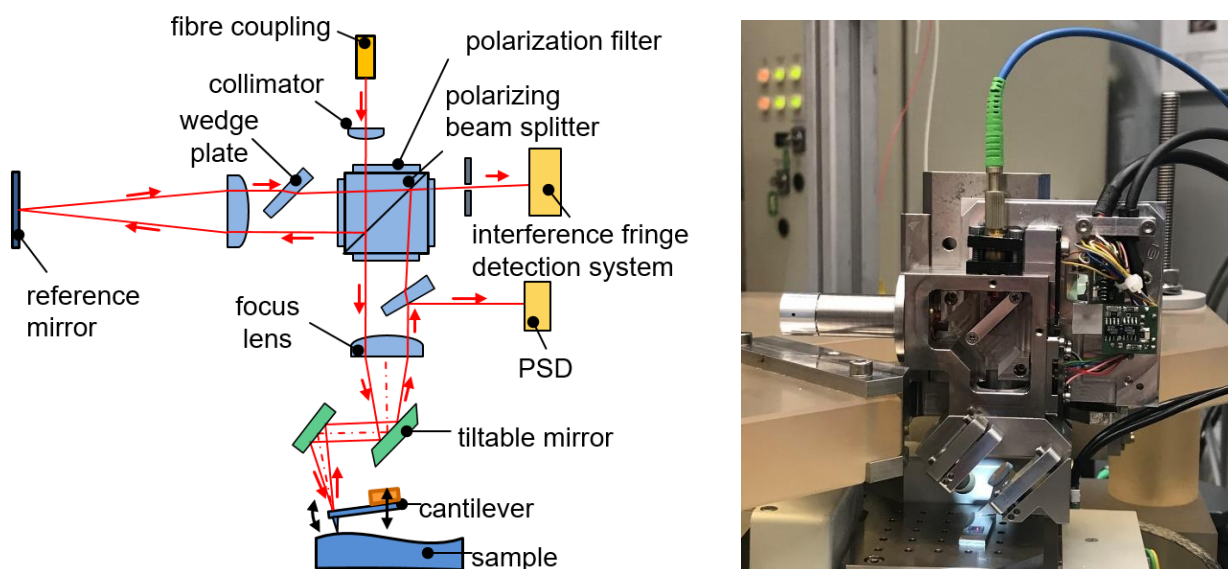


Figure 11. Optical AFM head, functional principle and realisation

FAU additionally constructed and manufactured a new AFM head for self-sensing cantilever to be integrated into NMM-1. Using that MAFM in a confidential project, a measurement with a scanning range of 10 mm by scanning speed 5  $\mu\text{m/s}$  was realised.

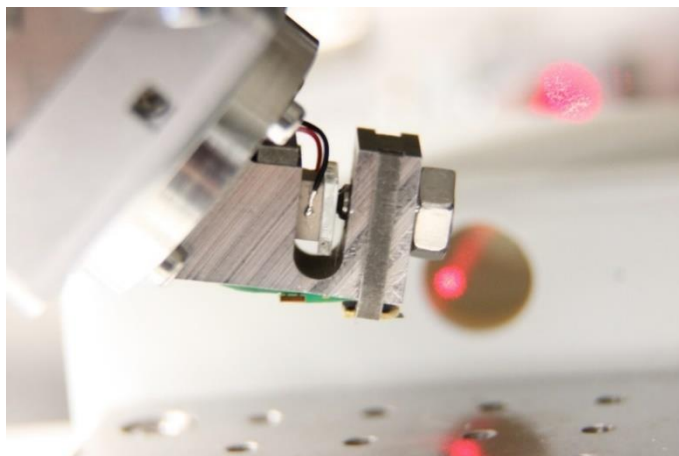


Figure 12. AFM head using self-sensing cantilever

#### 4.1.4 Summary of key research outputs

- **Mise en Pratique: realisation of the metre for nanometre and sub-nanometre scale applications**
  - Results from the bottom up approach and the x-ray interferometry work performed within this project have contributed to the realisation of the lattice parameter of silicon as a secondary length standard in the Mise en Pratique for the metre which was revised in May 2019.
- **New and improved measurement capabilities:**
  - A new bottom-up traceability approach was successfully developed and realised for determining the 3D dimension of complex nanostructures by using the lattice of crystal silicon as an internal ruler. The final measurement uncertainty budget indicates that the critical dimension (CD) of structures can be determined at a combined standard measurement uncertainty of 0.81 nm.
  - Various measures were successfully undertaken to improve the performance of MAFMs; i.e. to reduce the noise level to 0.1 nm (rms), to raise the scanning speed to 1 mm/s and extend the range to 25 mm.
    - PTB: by upgrading some key components for easier adjustment, better thermal behaviour and better stability, the noise level of the metrology tool was reduced significantly, for instance, the positioning noise along the z-axis has been improved from  $1\sigma = 0.52$  nm to  $1\sigma = 0.13$  nm. With the developments made, high-speed (*up to 1 mm/s*) and large range (*up to 25 mm*) metrological AFMs were successfully realised. Verification measurements indicate that the tool can calibrate the step height standards with a stability of better than 0.8 nm (p-v), and calibrate the pitch value of a 2D grating (nominal pitch of 1000 nm) with a stability better than 0.01 nm (p-v), when the measurement speeds are increased from 10  $\mu\text{m/s}$  to 1000  $\mu\text{m/s}$  (i.e. 100x times faster).
    - NPL: by installing a new scanning stage into its metrological AFM, the noise levels measured in the x, y and z axes were 0.25 nm, 0.55 nm and 0.31 nm. A further reduction is possible with more averaging of collected data to achieve the target of *0.1 nm rms*. Noise levels in NPLs' *high-speed* metrological AFM are between 0.1 nm and 0.4 nm depending on the mode of operation, the density of data points collected and the amount of averaging. Metrology was bought to a non-NMI high-speed AFM with the following results: an average speed in the fast axis approaching 9 mm/sec (higher than the target 1 mm/sec). The high-speed stage with a range of  $4\ \mu\text{m} \times 4\ \mu\text{m}$  is mounted on an x-y slip stick stage having a larger range (25 mm x 25 mm) and via a combination of movements an extended range of movement is possible.
    - FAU undertook various efforts to reduce the noise level of their NMM-1, which is used for the LR-AFM. In addition, FAU constructed and manufactured a new AFM head for self-sensing cantilever to be integrated into NMM-1. With that self-sensing AFM on the NMM-1, a noise level of 7 nm is reached (z-axis), which can be improved to 0.2 nm by filtering. Using the self-sensing MAFM in a confidential project, a measurement with a scanning range of 10 mm by scanning speed 5  $\mu\text{m/s}$  was realised
    - VSL demonstrated 0.1 nm rms noise level for their 3D AFM

- VTT redesigned its MAFM for 3D measurements and updated software to reduce noise level and to achieve a larger measurement range. A maximum measurement volume of  $(950\ \mu\text{m}) \times (950\ \mu\text{m}) \times (115\ \mu\text{m})$  and a noise level of 0.2 nm in interferometric measurements of the Z-direction were achieved.

## 4.2 Development of reference materials for 3D nanometrology tools

Reference materials and standards are widely used to calibrate, test and verify industrial equipment. Existing nanoscale standards such as step height and lateral 1D/2D gratings may in some cases satisfy industrial needs for scale calibration. Moreover, tip characterisers have been available for characterising probe geometries but they lack the accuracy needed by industry. To overcome these limitations, the project designed, manufactured and characterised new Line Edge Roughness (LER) and Line Width Roughness (LWR) reference materials, new Critical Dimension (CD) standards and new tip characterisers. The target uncertainty for the reference materials was  $< 1\ \text{nm}$ .

### 4.2.1 Design and production of reference materials

Based on the outcome of a survey among stakeholders done early in the project, several approaches have been followed to design and manufacture novel standards and prepare standards from existing nanomaterials. Consortium partners TNO and NCSR-D have used their production facilities to design and initially produce test samples that were evaluated by the NMI consortium partners. From these evaluations, process parameters and sample layouts were adjusted to improve the quality of the samples that were again evaluated as part of the comparison activity by the NMI partners.

SMD prepared nanoparticle samples from commercially available sources. Also, here a preliminary test run was produced to be evaluated by the NMI partners in order to provide feedback to SMD for process optimization. Optimized sets of samples were finally distributed as part of the comparison activity.

INRM prepared tobacco virus samples that were distributed within the consortium. PTB distributed a line width standard for critical dimension (CD) measurements.

#### The Siemens star standard

The Siemens star concept provided structures with multiple angular positions that would enable probe shape reconstruction along various profiles. The accuracy of the probe reconstruction would be determined by the smallest details at the centre of the star. The overall micrometre sized shape was intended to be studied as a scatterometry and hybrid metrology standard.

The final design of the Siemens star sample is shown in Figure 13. The sample provided multiple regions with identical fields and within each field a set of stars with different geometrical properties. Both the number of spokes in the stars and the gap within the centre region vary within each field in order to select the best configuration for each application.

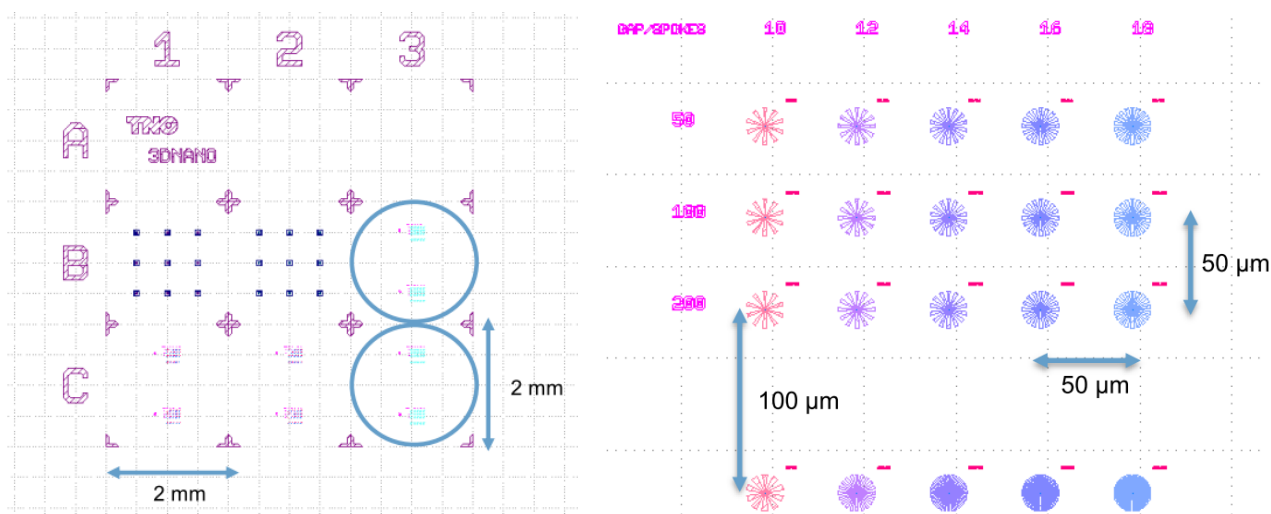


Figure 13. Final design of the Siemens star sample with an overview (left) and detail of the actual star region (right) providing multiple standards with different geometrical properties

#### The nanoparticle standards

SMD made a selection of commercially available nanoparticle systems that could be useful as reference materials. The selection initially contained two different diameters mono disperse spherical gold, mono disperse silver and mono disperse silica nanospheres and non-spherical gold nanorods. Sample sets for evaluation were prepared by SMD by depositing the particles on a mica substrate. These sample were distributed to CMI, NPL and VSL for additional evaluation. Based on these evaluation results it was concluded that the preparation procedure of the samples was satisfactory and could therefore be used to prepare the final batch for distribution within the consortium. The final batch was prepared for four nanoparticle systems listed in Table 1.

Table 1. Nanoparticle systems selected for the final batch that was circulated within the consortium.

Nanoparticle sample ID	Type	Supplier	Specifications (nominal mean size $\pm$ SD)
Np1	Gold nanospheres	NIST (RM8012)	Diameter = $(24.6 \pm 1.1)$ nm
Np2	Gold nanorods	Nanocomposix	L= $(58.4 \pm 4.4)$ nm, W= $(15.5 \pm 1.4)$ nm, AR 3.8
Np3	Silver nanospheres	Nanocomposix	Diameter = $(48.0 \pm 5.0)$ nm
Np4	Silica nanospheres	IRMM FD304	Diameter = $(27.8 \pm 1.5)$ nm

#### The nanopillar array standard

NCSR-Demokritos developed an alternative process approach for the fabrication of nanopillar samples. Instead of etching the silicon substrate, a silicon substrate with a 100 nm silicon oxide overlayer was used and processed. This new approach provided the following improvements over the former process:

- Optimal etch process control over the nanopillars' height. The depletion of Si oxide (in bulk) during RIE was monitored in real time via interferometry. It was therefore impossible to under-etch and in case of moderate over-etching, pillar height was kept constant and equal to the thickness of the pre-determined Si Oxide layer. Plasma selectivity also offered stable etch rates, since these were unaffected by substrate/pattern area (macro-loading effects); any ambiguity about pillar height was, thus, lifted.
- Optimized pillar profile. Thanks to plasma anisotropy, lateral etch rates were kept to a minimum. Pillars assumed an overall optimised profile with higher contrast and near vertical sidewalls. We may also have observed a mitigation of short range proximity effects, as those previously manifested in the shape of resist filaments, resist accumulation between pillars etc.

In Figure 14 is show the comparison between the results for the former production process that yields silicon nanopillars and the improved process that resulted in silicon oxide pillars. Both samples were designed for a pillar height of 100 nm, a pillar diameter of 50 nm and a pitch of 100 nm. The SEM cross sections show better uniformity of the height and steeper side walls for the improved process.

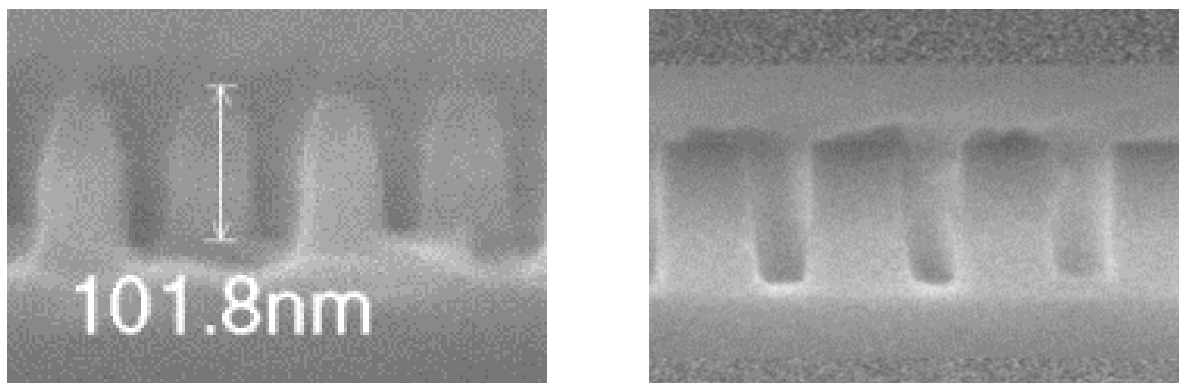


Figure 14. Results of the former nanopillar production process (left) and the improved process (right) illustrating improved uniformity of the pillar height and steeper side walls for the improved process.

The improved production process was finally used to manufacture two nanopillar array samples of similar layout, Figure 15, that were distributed within the consortium for evaluation.

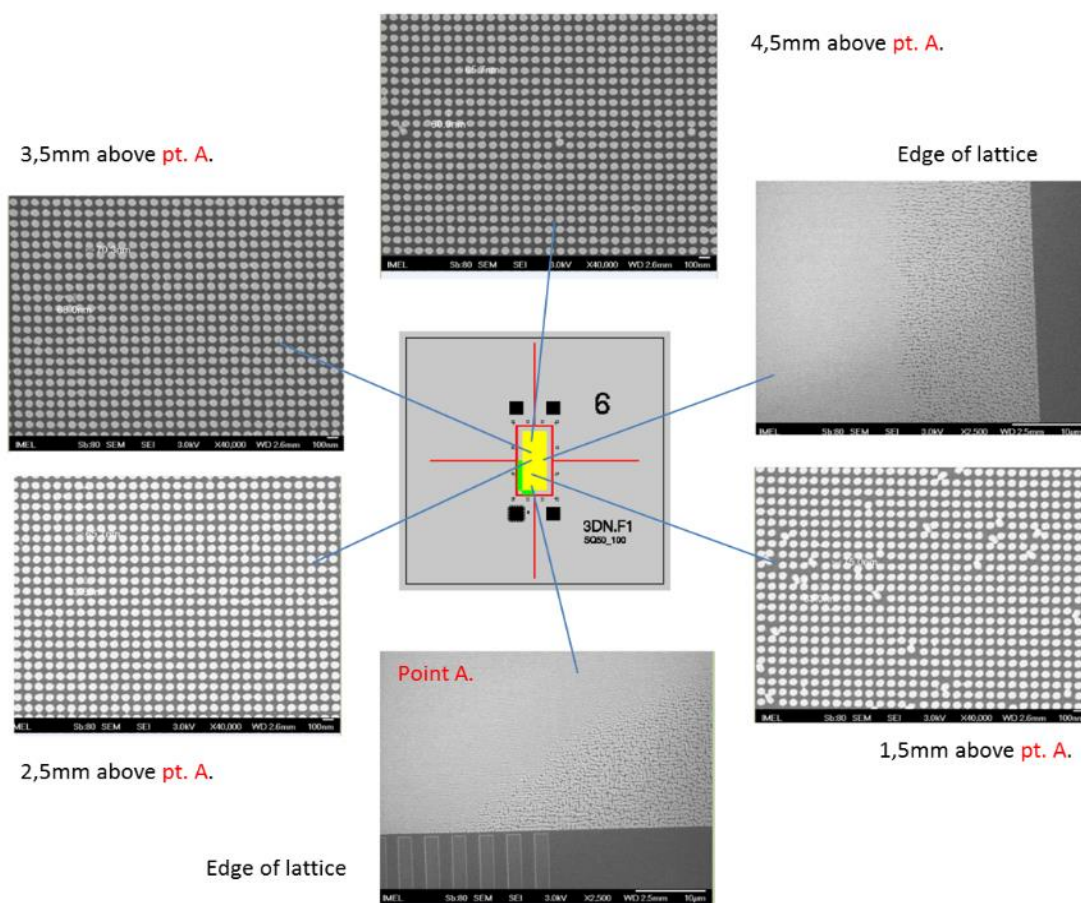


Figure 15. Overview and details of NCSR-Demokritos of one of the nanopillar array samples, S3DNF1\_6

#### 4.2.2 Characterisation of reference materials

Measurements on the TNO Siemens star, NCSR-Demokritos nanopillar samples, SMD nanoparticle samples and INRIM Tobacco virus sample were mainly performed by AFM. Additional measurements by scatterometry, Mueller polarimetry and ptychography were selectively performed by DFM and VSL.

Agreement was obtained on the relevant measurands for the individual standards, Table 2. A measurement protocol was drafted by VSL incorporating input from various partners to be used as a guideline for the measurements.

Table 2. Proposed measurands for the various standards.

Standard	Measurands
Siemens star	Height, Side wall angle (SWA), Line edge roughness (LER), line width roughness (LWR), maximum spoke angle error, Sq roughness on upper and lower level
Nanopillar	Height, horizontal and vertical pitch, pillar diameter and SWA.
Nanoparticles	Diameter, length, width and aspect ratio only for the nanorods
Tobacco Mosaic Virus (TMV)	Height, diameter

#### Siemens star results

Comparison reports for the Siemens star standard were obtained by DFM, METAS, NPL and VSL. All samples were produced by TNO using the same process settings to maximize the similarity of the samples except for the samples measured by CMI. A single sample with identification 'Etch test #3' was measured both by DFM and VSL on the exact same features. A selection of the results is shown in Table 3 and

Table 4. Results for the VSL AFM measurements on the same Siemens star features

Table 3. Results reported by DFM for the Siemens star standard

Sample ID Etch test #3	C-3-1-18-50		C-3-1-18-100		C-3-1-18-200		C-3-1-16-200	
Quantity	Mean	STD <sup>1)</sup>	Mean	STD	Mean	STD	Mean	STD
Height (nm)	64.09		63.74		63.75		63.69	
Side wall angle X <sup>2)</sup> (degree)	74.06	1.53	67.53	2.32	69.63	2.89	65.43	2.23
Side wall angle Y (degree)	79.07	1.39	83.83	2.18	80.95	2.24	76.97	3.74
Line edge roughness, LER <sup>3)</sup> (nm)	8.66	2.01	8.01	1.90	7.51	2.03	9.20	2.37
Line width roughness, LWR (nm)	16.00	3.70	15.14	3.51	13.52	3.92	16.96	1.12
Max. spoke angle error (degree)	0.33	0.61	0.52	0.73	0.47	0.74	1.12	0.76
Sq roughness lower level (nm)	0.19	0.05	0.30	0.04	0.22	0.01	0.19	0.03
Sq roughness upper level (nm)	0.26	0.02	0.19	0.02	0.17	0.01	0.25	0.03

- 1) STD = standard deviation of repeated measurements. Number of measurements is five except for LER, LWR and angle error, which are 2x, 1x and 1x number of spokes, respectively.
- 2) Side wall angle is reported as the mean of the side wall angles of the left and right side.
- 3) For LER, LWR and angle error analysis, outliers due to particle contaminations have been excluded.

Table 4. Results for the VSL AFM measurements on the same Siemens star features

Sample ID Etch test #3	C-3-1-18-50		C-3-1-18-100		C-3-1-18-200		C-3-1-16-200	
Quantity	Mean	STD <sup>1)</sup>	Mean	STD	Mean	STD	Mean	STD
Height (nm)	59.91	0.04	59.83	0.53	59.67	0.03	60.22	0.16
Side wall angle <sup>2)</sup> (degree)	81.4	0.3	81.7	0.7	80.1	2.4	70.1	5.2
Line edge roughness, LER (nm)	4.48	1.51	4.17	1.20	3.32	0.88	4.69	3.92
Line width roughness, LWR (nm)	6.24	0.53	6.34	0.39	4.94	1.17	7.25	4.18
Max. spoke angle error (degree)	7.3	2.2	7.3	2.2	6.2	2.0	7.5	2.4
Sq roughness lower level (nm)	0.90	0.14	1.16	0.52	0.81	0.01	0.99	0.38
Sq roughness upper level (nm)	0.60	0.13	1.20	0.55	1.07	0.21	0.92	0.34

- 1) STD = standard deviation of repeated measurements. Number of measurements is four except for LER, LWR and angle error, which are 2x, 1x and 1x number of spokes, respectively.
- 2) The side wall angle is calculated as the average over all spokes corrected for the opening angle of the probe.

The uncertainty calculation for these measurands was mostly based on the repeatability of the measurement results. In some cases, the uncertainty was not reported making a comparison of results less valuable. Nevertheless, the results for the Siemens star measurements show reasonable agreement for some measurands (roughness, height, side wall angle) but large differences for others like the spoke angle error. This can probably be attributed by the measurement and analysis procedures.

#### Nanopillar array results

NCSR-Demokritos manufactured two square lattice nanopillar samples that were measured by VSL and CMI. A commercially available less dense pillar sample was purchased by DFM and measured by AFM and Mueller polarimetry. These results are described in the Hybrid Metrology section.

The measurements by VSL were performed with different probe types in order to investigate the effect of the probe shape on the results. From the measurements on the nanopillar array, the AFM probe radius was estimated and subsequently used to compensate the calculation of the pillar width.

Table 5. VSL AFM measurement results for the nanopillar array S3DNF1-6

Sample S3DNF1-6								
probe type	Height		Xpitch		X diameter		Comp X diameter	
	Mean	std	mean	Std	mean	std	mean	std
	/nm	/nm	/nm	/nm	/nm	/nm	/nm	/nm
CNT-150	67.3	0.9	97.2	0.4	83.6	0.7	59.1	1.6
SSTrench	109.2	1.0	96.5	0.1	87.1	1.8	66.6	6.7
TESP-SS	106.7	1.2	99.5	0.1	91.6	1.7	70.8	3.2

Table 6. VSL AFM measurement results for the nanopillar array S3DNF1-7.

Sample S3DNF1-7								
probe type	Height		Xpitch		X diameter		Comp X diameter	
	mean	std	mean	Std	mean	std	mean	std
	/nm	/nm	/nm	/nm	/nm	/nm	/nm	/nm
SSTrench	50.8	0.7	96.7	0.4	86.3	2.3	20.5	15.1
TESP-SS	108.9	1.5	98.4	0.3	89.3	5.5	72.6	4.5

The results obtained by CMI are given in Table 7. Two different probe types were used. The results have not been corrected for the probe shape. The pillar diameter has been evaluated as an effective diameter for the areas selected at 85 % threshold.

Table 7. CMI AFM measurement results for the nanopillar array S3DNF1-6.

Sample S3DNF1-6				
probe type	Height		Diameter	
	mean	std	mean	std
	/nm	/nm	/nm	/nm
rtespa150	101.7	–	38.40	1.33
TESP-SS	102.8	–	40.82	0.82

The small pitch and high density of the nanopillar array hampered the accessibility of regions in between the pillars. This was especially visible in the VSL result for the CNT-150 probe on sample 6 and the SSTrench probe on sample 7; the lower level in between the pillars could not be reached by these probes, resulting in an erroneous height value. The remaining height values are similar to the CMI results although the uncertainty (stated as a standard deviation) for the CMI results was not given. The pillar diameter depends critically on either the accuracy of the probe shape correction (for VSL) or the selected threshold value to include the relevant data (for CMI). The large deviations in the corrected pillar diameter for the VSL results indicate that the probe shape correction is not accurate for this sample.

### TMV results

The Tobacco Mosaic Virus (TMV) samples to be imaged by AFM were prepared on cleaved mica by depositing a few drops of purified and diluted suspension of TMV in water and let them to dry in air. As a general remark, a quite good stability of the TMV samples deposited on mica was observed over long time intervals.

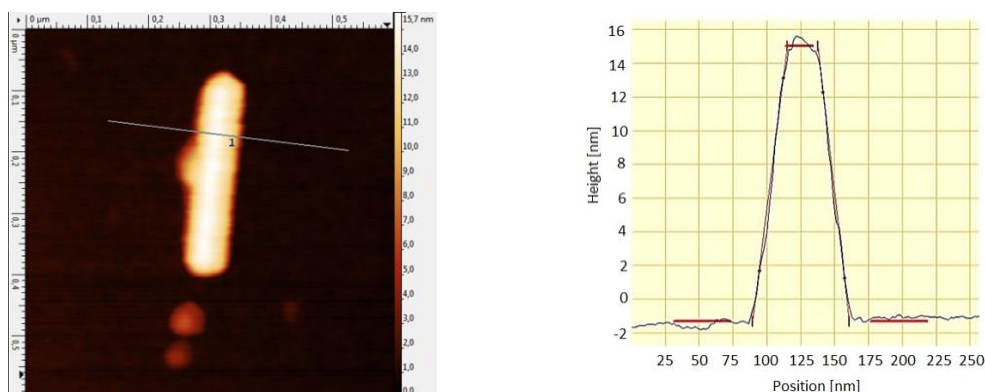


Figure 16. AFM image (a) and 2D profile (b) of a TMV on mica.

A diameter of about 18 nm by X-ray fiber diffraction of the rod-shaped TMV has early been reported in literature. By the AFM the diameter of the TMV is determined as the top-height of the rod from the reconstructed profile of isolated virions. The mean diameter of the rod resulting from the top-height reconstruction of several virions and different tips is of about 16.5 nm with a standard deviation of 1.0 nm. Among others, the interactions between AFM tip, virion and mica substrate have been investigated with reference to experimental data and models in literature in order to determine deformations and associated uncertainty of corrections, by which a better agreement between the top-height diameter and reference value is achieved. Elastic tip-sample interactions and sample-substrate adhesive deformations have been determined by the classical Hertzian and Maugis-Pollack models. An uncertainty budget has been estimated for the top-height measurements including uncertainties of corrections.

### Hybrid metrology results

In order to explore the potential of the standards for hybrid metrology, the Siemens star sample and nanopillar sample were measured both by AFM and scatterometry, ptychography and polarimetry. A Siemens star sample was measured at VSL both by AFM and ptychography. The development of the analysis software for ptychography is still in progress so currently only the equivalent of a height could be generated. A comparison between the AFM and ptychography results is shown in Figure 17.

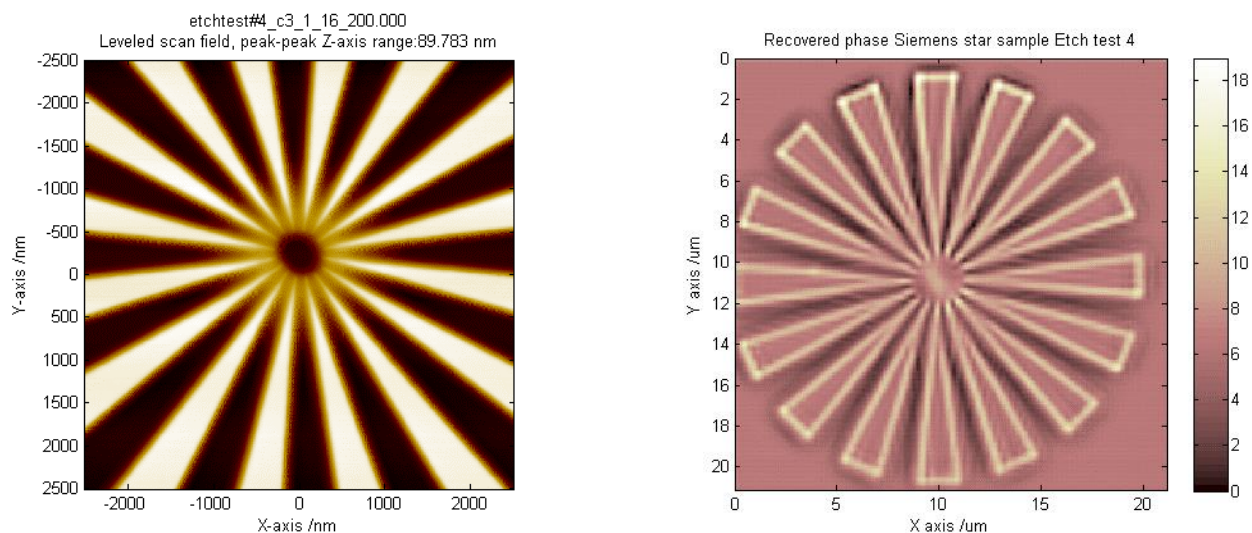


Figure 17. AFM and ptychography results on the same Siemens star feature.

The height measured by AFM is 77 nm while the reconstructed phase (proportional to the physical height) for the ptychographic data corresponds to a height of about 20 nm. Additionally, the phase profile is not flat over the spokes as would be expected but enhanced. This effect and the large discrepancy from the AFM result require further research.

DFM has studied a commercially available nanopillar sample before the NCSR-Demokritos samples became available. The sample used in this study is from Eulitha and labelled P200s\_5w5. Similar to the NCSR-Demokritos samples, these are two-dimensional array gratings. The period of the grating is 200 nm in both directions. The nominal height of the grating is 100 nm with a nominal width of 80 nm. The sample was measured with scatterometry, ellipsometry and AFM. The quality of the model fit to the measurement data improved for the ellipsometric parameters  $\rho$  and  $\Delta$  and the scatterometric diffraction efficiency  $\eta$  when the AFM data is included, Figure 18.

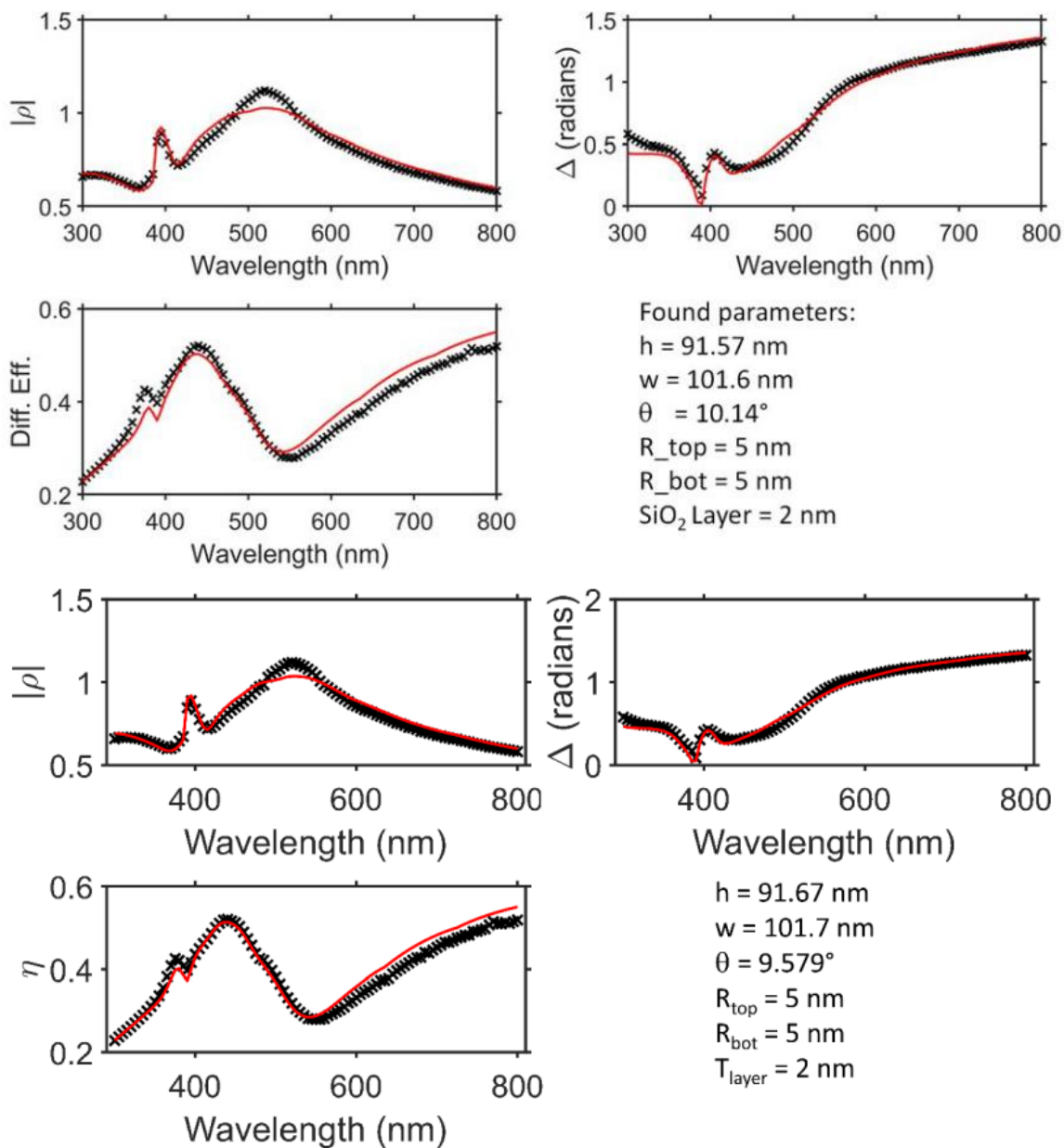


Figure 18. Ellipsometry and scatterometry results without (top three graphs) and with (bottom) additional information from AFM measurements.

Nanoparticle results

Nanoparticle samples, prepared by SMD, were distributed to DFM, INRIM, METAS and VSL. A representative selection of the results is given in **Error! Reference source not found.** and **Error! Reference source not found.**

Table 8. Reported results from DFM for the AFM measurements on the nanoparticle samples.

Sample	Particle sample	Nominal diameter (nm)	$D_{\text{mean}} \pm SD$ (nm)	$u_c$ (nm)	$N$
Np1	Gold nanospheres	$24.6 \pm 1.1$ nm	$24.7 \pm 2.6$ nm	0.7	394
Np3	Silver nanospheres	$48.0 \pm 5.0$ nm	$46.3 \pm 5.6$ nm	1.1	182
Np4	Silica nanospheres	$27.8 \pm 1.5$ nm	$24.8 \pm 2.6$ nm	0.8	119

Sample	Type	Nominal size (nm)	$W_{\text{mean}} \pm SD$ (nm)	$L_{\text{mean}} \pm SD$ (nm)	$u_c$ (nm)	$N$
Np2	Gold nanorods	L = $58.4 \pm 4.4$ nm, W = $15.5 \pm 1.4$ nm	$16.5 \pm 1.2$ nm	–	0.7	349

Table 9 Reported results from INRIM for the AFM measurements on the nanoparticle samples.

Sample	Particle sample	Nominal diameter (nm)	$D_{\text{mean}} \pm SD$ (nm)	$u_c$ (nm)	$N$
Np1	Gold nanospheres	$24.6 \pm 1.1$ nm	$24.8 \pm 1.3$ nm	0.9	50
Np3	Silver nanospheres	$48.0 \pm 5.0$ nm	$48.1 \pm 6.5$ nm	1.3	55
Np4	Silica nanospheres	$27.8 \pm 1.5$ nm	$25.6 \pm 2.1$ nm	1.0	45

Sample	Type	Nominal size (nm)	$W_{\text{mean}} \pm SD$ (nm)	$L_{\text{mean}} \pm SD$ (nm)	$u_c$ (nm)	$N$
Np2	Gold nanorods	L = $58.4 \pm 4.4$ nm, W = $15.5 \pm 1.4$ nm	$15.5 \pm 0.8$ nm	–	0.9	45

The results for the nanoparticle were generally in good agreement with uncertainties in the nm range.

#### Probe radius reconstruction capability

In order to investigate the potential of the developed materials as a 3D AFM probe shape reconstruction tool, the developed standards were measured under the same conditions (i.e. scanning area, setpoint and speed) with the same probe. Since this experiment required a substantial amount of measurements and a new probe would suffer from wear during the experiment, a worn probe was used to limit the amount of additional wear during the experiment. Next to the measurements on the developed standards, additional measurements were performed on three types of commercially available standards and a VSL sample with spherical nanoparticles, Table 10.

Table 10. List of standards used for the probe shape recovery investigation.

Material	Features	Specifics
NCSR-D Nanopillar	Dense array of silicon pillars	Hexagonal and rectangular
TNO Siemens star	Silicon star structure	Variable width, multiple angles
SMD Nanoparticle sample 1	Gold nanospheres	Mono disperse
SMD Nanoparticle sample 2	Gold nanorods	Non-spherical
SMD Nanoparticle sample 3	Silver nanospheres	Mono disperse
SMD Nanoparticle sample 4	Silica nanospheres	Mono disperse
VSL Nanospheres sample	Poly-styrene nanospheres	Wide diameter distribution
Aurora Nano devices NioProbe	Nano rough surface	Limited feature height
NT-MDT TGT1	Low density spikes	Spike angle 30°
NT-MDT TGX1	2D grating	Square undercut structures

All measurements were pre-processed and analysed with equal settings of the processing and analysis software to minimize the influence on the consistency of the probe radius determination. The analysis was based on blind reconstruction, except for the VSL sample. The VSL measurements were processed with a proprietary method based on the assumption that the nanoparticles are indeed spherical such that any non-sphericity of the raw data is caused by the probe shape. Each spherical particle is therefore fully described by the particle height while height can be measured accurately by AFM. Consequently, the probe shape can be recovered by subtracting the spherical shape for each measured particle. This method is considered traceable in contrast to blind reconstruction and is used in this investigation as a reference result.

The blind reconstruction result for the other materials also yields a 3D shape, Figure 19. The probe radius was determined by fitting a sphere to the upper part of the 3D shape.

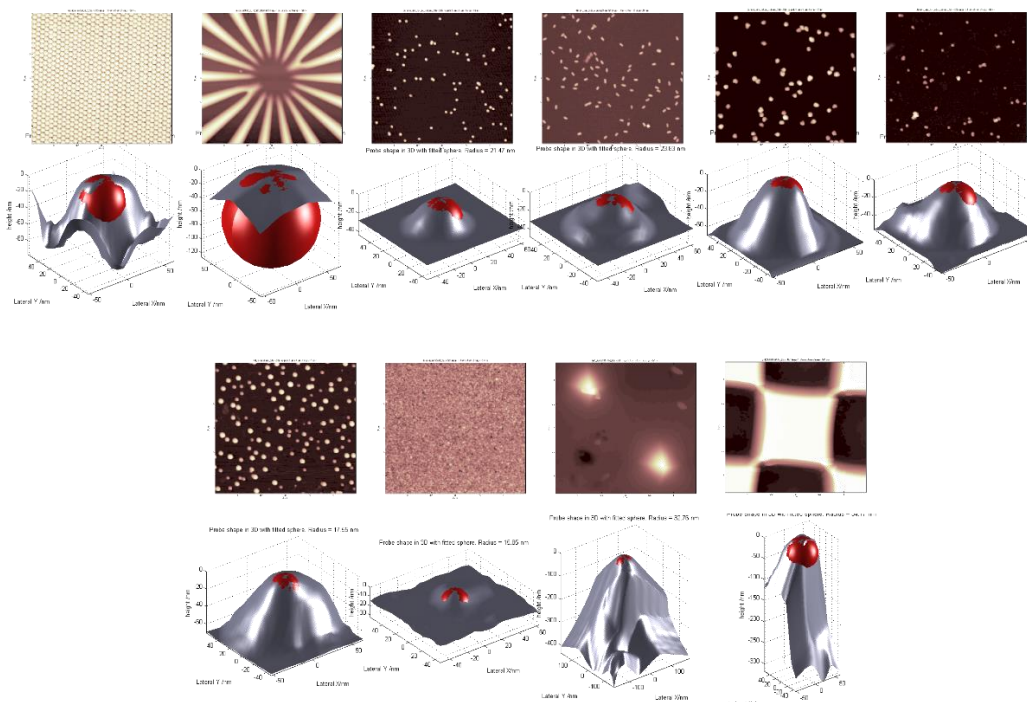


Figure 19. AFM measurements on the various standards in the order of Table 10 from the upper left to lower right. Below each AFM result is the 3D shape obtained from the blind reconstruction method except for the VSL nanospheres sample (lower left).

The results of the probe radius determination are shown in Figure 20. The results are mostly in agreement. The error bars represent twice the standard deviation of the results. The nanopillar result is probably influenced by the fact that the array is very dense so that the probe can't reach the intermediate regions. The lack of very small features in the Siemens star limits the blind reconstruction outcome and results in a larger radius compared to the other results. This is also the case for the TGT1 and TGX1 material. The SMD nanoparticle results show internal consistency and good agreement with the reference value of the nanospheres.

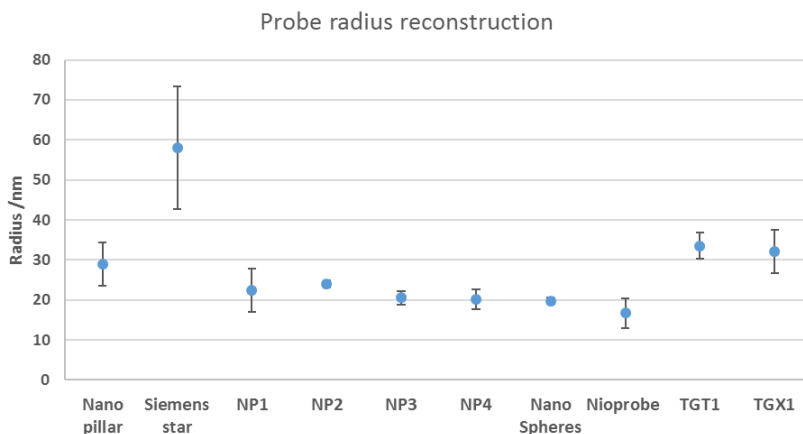


Figure 20. Analysis results for the probe radius reconstruction potential.

#### 4.2.3 Summary of key research outputs and conclusions

- **Dissemination**

A paper titled "Progress on the development of reference standards for 3D nanometrology" combining the project's work performed on the 3D standards was prepared and submitted for publication in Measurement Science and Technology

- **New measurement capabilities**

There are currently no CMC entries for line width, line edge roughness, line width roughness and side wall angle and probe radius calibration. All measurements performed in this activity therefore provide a basis for new measurement capabilities for these measurands.

- **New reference materials, reference methods, procedures developed.**

The development and characterization of the Siemens star, nanopillar array and nanoparticle standards shows good potential for new reference standards for AFM and/or optical measurement methods. Especially the pillar array and nanoparticle samples show reasonable agreement when used as an AFM probe characterizer. The target uncertainty of less than 1 nm was achieved for some of the measurands and reference materials, e.g. the results for the nanoparticle were in good agreement with uncertainties in the nm range. The process results for the Siemens star currently lack sufficiently small features for AFM applications but could still be useful as an optical standard. Novel procedures have been developed and shared to measure the samples and analyse the results.

The effort to manufacture the Siemens star standard and the nano-pillar array standard is quite substantial and require dedicated facilities. These standards are therefore mainly intended for use at the NMI/DI level. The preparation of the nanoparticle standards is much less complicated and be scaled quite easily. These standards would be suitable for use in all sectors from NMI/DI to the wider industry.

- **Key technical insights gained**

The consistency of results obtained from the NMI partners could still be improved. Although there are sample-to-sample differences due to fabrication tolerances, harmonized measurement and analysis procedures would help to improve the comparability of results. The uncertainty estimate of most results from the NMIs was given as standard deviations from the measured values. Since this is only one contribution, although an important one, to the total measurement uncertainty, the further development of task specific uncertainty budgets is needed to improve the comparability of results.

### 4.3 Widening the understanding of probe-sample interactions in AFM and SEM measurements

Understanding probe-sample interactions is a key for improving measurement uncertainty. Prior to the start of the project, AFM tip probe-sample interaction studies were limited to measurements of nearly flat surfaces, only. The project developed models for true 3D measurements. Critical issues such as structure/tip deformation due to the measurement force and humidity were theoretically and experimentally studied. Moreover, a special reference material was developed to improve the metrological characterisation of the AFM probe, and the simulation of SEM measurements included a physical model of SEM image formation of nanodimensional reference structures for the quantitative analysis of SEM images for CD and shape metrology. Finally, the impact of SEM image noise on line edge roughness measurements was investigated.

#### 4.3.1 Probe-sample interaction force

NPL developed reference probes and samples to perform novel types of experiments for probe-sample elastic deformation analysis at CMI. The samples for determining the probe-sample deformation in different scanning regimes consist of a set of chromium patterns on glass and silicon (see Figure 21). These were measured using different methods, coated by additional chromium layer to get homogeneous surface material and measured again. The probes for determining the lateral probe-sample deformation were manufactured using electron beam induced deposition method. A special set of probes with very high aspect ratio and with different cantilever stiffnesses was developed to reach different ranges of cantilever torsion and probe deformation.

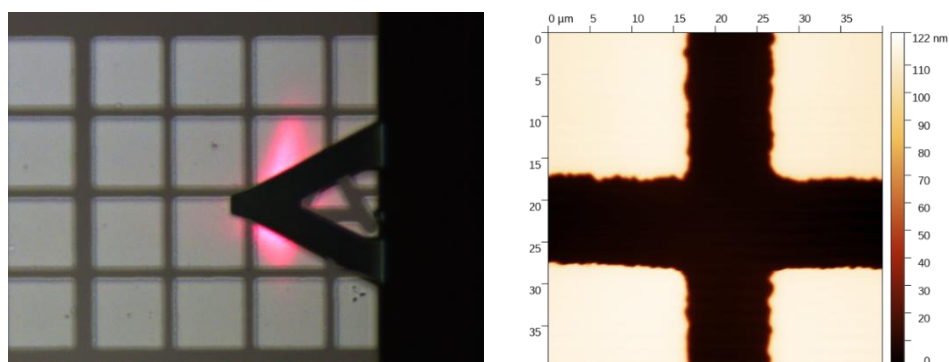


Figure 21. Chromium on glass reference sample and its topography.

To study the probe-sample interaction, the reference samples were complemented by other typical SPM samples, including nanoscale roughness on silicon, quantum dots (see Figure 22) and step height patterns. By measurements with varying contact forces the effect of probe and sample compliance on the measured parameters were investigated.

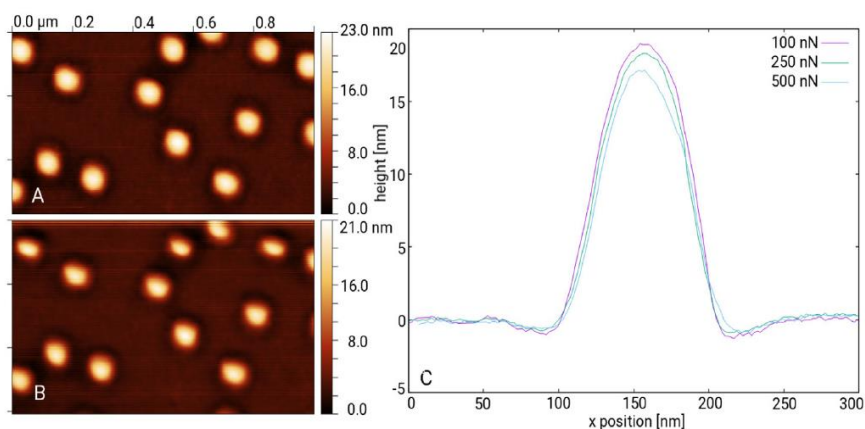


Figure 22. Changes in topography of a quantum dot sample measured using different contact forces. The effect is repeatable, i.e. reducing the contact force leads to the original shape. See Ref. C1 for more details.

To measure the impact of lateral forces on probe deformation and cantilever torsion a probe-on-probe technique was developed allowing to distinguish the two effects and to estimate the sensitivity of torsional microscope signal on the probe apex lateral shift.

#### 4.3.2 Data analysis of AFM data

To analyze the impact of probe-sample elastic deformation on SPM data novel methods were developed. The simplest approach is to use Hertz model for locally fitted curvature of the probe and sample, which can be done using a special data processing module in the open source software Gwyddion. Such method is suitable for a quick estimate of the potential probe and sample deformation for particular contact force. For a more accurate estimation, we need to work with the real probe and sample shape. This could be done using Finite Element analysis; however this would be too slow for a pixel by pixel simulation of the probe-sample interaction during the SPM scan. Therefore, we have developed a simplified method based on a spring mass model allowing to get the mechanical results with about 10 percent accuracy in time scale at least an order of magnitude shorter. This is based on use of Gwyddion software for creating a regular rectangular mesh from the measured, simulated or estimated probe and sample geometry and running a mass-spring solver on this mesh, for different probe positions on the sample (see Figure 23).

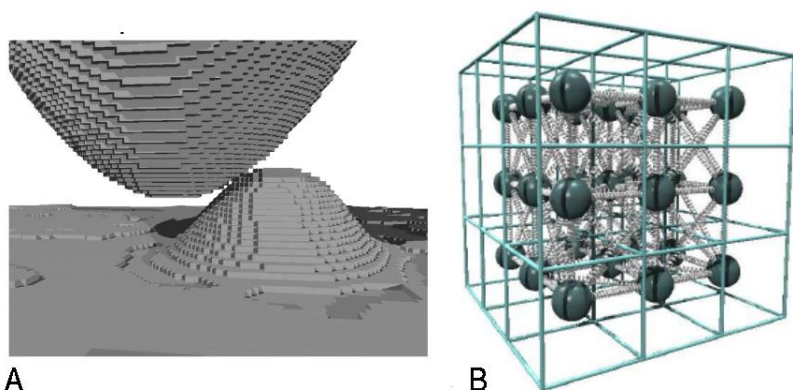


Figure 23. Construction of the regular mesh from probe and sample geometry and construction of the mass-spring model from these data. See Ref. C1 for more details.

The mass spring model was used to analyse the impact of elastic probe-sample interaction on the measured topography and compared with experimental data on different samples. As an example, the quantum dot measurement result is shown in Figure 24. It was shown that the calculated probe and sample elastic deformation are typically underestimated, which might be caused by other elements that relax, namely the cantilever that undergoes torsion. This effect was studied separately in the project to get a complete view on the different elastic deformation mechanisms.

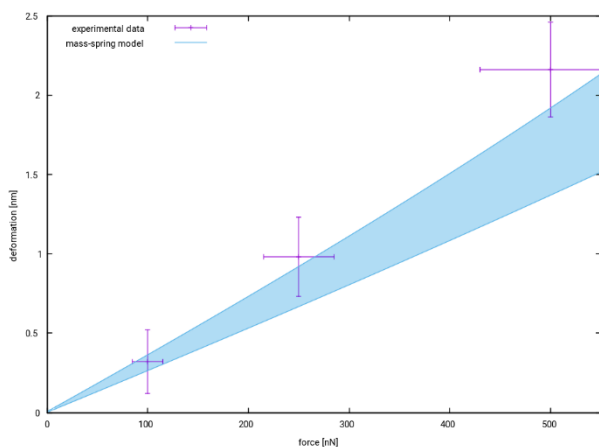


Figure 24. Results of the mass-spring model calculation compared with experimental data, uncertainties added to both numerical and experimental results. See Ref. C1 for more details.

- [C1] P. Klapetek, A. Charvátová Campbell, V. Buršíková, "Fast mechanical model for probe-sample elastic deformation estimation in scanning probe microscopy", *Ultramicroscopy* **201**, 18–27 (2019).
- [C2] E. Anguiano and M. Aguilar, "Cross measurement procedure (cmp) for noise free imaging by scanning microscopes", *Ultramicroscopy* **76**, 39–47 (1999).

### 4.3.2 Role of humidity in SPM measurements

The project studied experimentally the effect of humidity level on the probe-sample interaction of AFM in order to improve instrumentation and interpretation of measurement results. Two different experimental set-ups to study the effect of humidity on AFM measurements were developed at DFM and SMD.

At DFM a simple environmental control was built on a Bruker Multimode 8 with PeakForce tapping. The environmental conditions can be modified by heating the sample stage and by the injection of various gas in the chamber such as nitrogen. The flushing of the chamber with nitrogen allows to reduce the humidity level. At SMD an Asylum Research MFP3D Infinity AFM instrument has been installed in a walk-in climate chamber. The temperature in the chamber can be controlled from  $-10\text{ }^{\circ}\text{C}$  to  $60\text{ }^{\circ}\text{C}$  and the relative humidity from 10 % to 95 %. The AFM enclosure and the climatic chamber are equipped with calibrated sensors allowing to monitor the environmental conditions.



Figure 25. Experimental set-ups used for humidity measurements left DFM right SMD.

### Results

Two sample specimens were studied at DFM: a 25 nm nominal stepheight from NT-MDT (Figure 26 left) and 100 nm nominal NIST polystyrene nanospheres deposited on mica substrate (Figure 26 right). The samples were measured by PeakForce tapping using Nanosensors PPP-NCST probes (7.4 N/m). The samples were continuously scanned for 1 hour before acquisition to stabilize the environmental conditions of the experiment. The humidity level was reduced by purging the chamber with nitrogen.

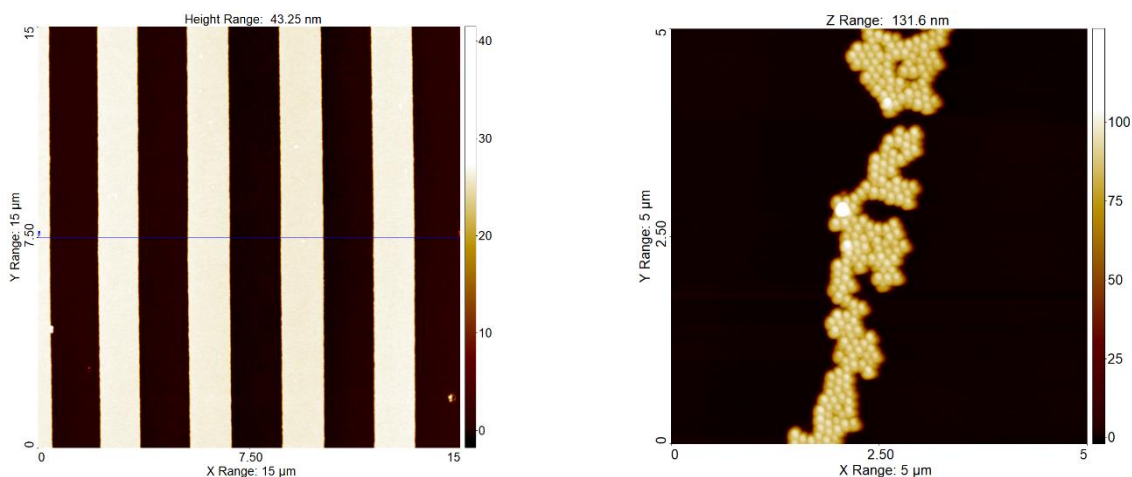


Figure 26. AFM image of the topography of the NT-MDT stepheight sample (left) and the NIST nanoparticle sample (right).

The stepheight was characterized by measuring the height on the steps following the ISO5436 standard. The nanoparticles were characterized measuring the maximum height relative to the background substrate. The results obtained for different relative humidity level while maintaining a constant temperature are presented in Table 11. The relative humidity was reduced from 30.42 % for the stepheight and 26.07 % for the nanoparticles to almost 0 %. In both cases the measured heights of the samples were constant and not affected by the humidity level.

Table 11. Measurement of the height of the NT-MDT stepheight and the diameter of the NIST nanoparticles at different relative humidity levels.

Sample	RH (%)	T (°C)	Mean height (nm)	SD (nm)
NT-MDT stepheight	<b>30.42</b>	30.52	26.22	0.06
	<b>0.10</b>	29.92	26.15	0.06
NIST nanoparticles	<b>26.07</b>	31.57	93.94	4.62
	<b>0.10</b>	31.07	93.38	4.70

Two sample specimens were studied at SMD: a 44 nm nominal stepheight from VLSI (Figure 27 a) and IRMM FD304 silica nanoparticles deposited on mica substrate (Figure 28 a). The samples were measured by tapping Mode AFM using Olympus OMCL AC240TS probes (1.5 N/m). In the case of the stepheight sample, the sample was continuously scanned while varying the environmental conditions and the measurements were performed on the same location. For the nanoparticles, the AFM probe was kept in contact with the sample during the modification of the environmental conditions to limit tip wear. A new fresh area close to the stabilization contact point was measured. The acquisition of the images was performed after stabilization of the temperature and relative humidity. Images were recorded at low scan speed (0.4 Hz) and at reduced tapping force (amplitude setpoint/free amplitude > 85 %).

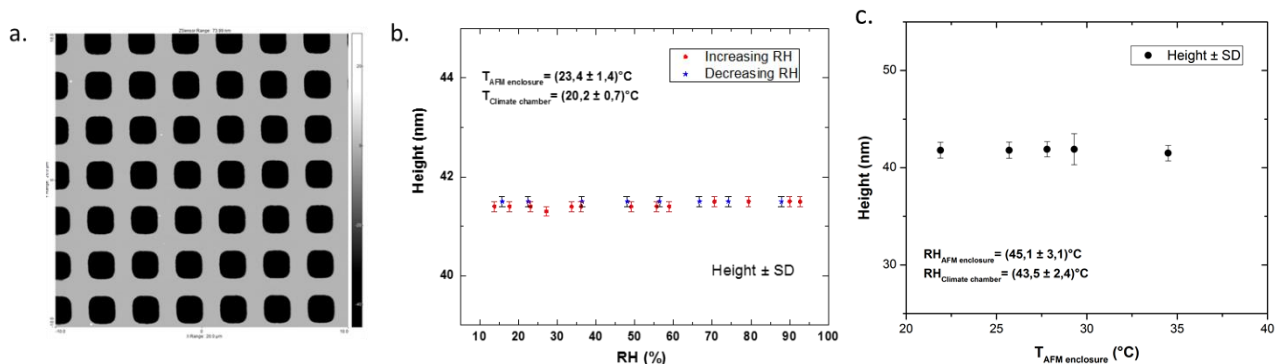


Figure 27. An example of a  $20 \times 20 \mu\text{m}^2$  AFM image of the topography of the VLSI stepheight sample (a). Measured mean height using ISO5436 standard for different humidity levels (b). Measured mean height for different temperature and constant humidity (c).

The environmental conditions were measured with calibrated sensors in the climate chamber and in the AFM acoustic enclosure close to the sample. It should be noted that the temperature is a few degrees higher in the AFM enclosure due to the heat induced by the AFM electronics. The reported value in the data are the environmental conditions close to the sample.

The measurements on the VLSI step height sample are reported on Figure 27. The relative humidity was increased from 10 up to 93 % and then decreased to the starting value while keeping the temperature constant (Figure 27 b). The heights of the step height were measured following the ISO5436 standard. The measured height is  $41.4 \pm 0.1$  nm (at 13.8 % of relative humidity) and does not vary for each relative humidity level considered. The measurement is not affected by the variation of the humidity level.

The temperature was then increased from about 20 °C up to 35 °C while keeping the relative humidity constant (Figure 27 c). The temperature was not increased higher than 35 °C to avoid damaging AFM electronics. The measured height of the sample was not affected by the increase of the temperature.

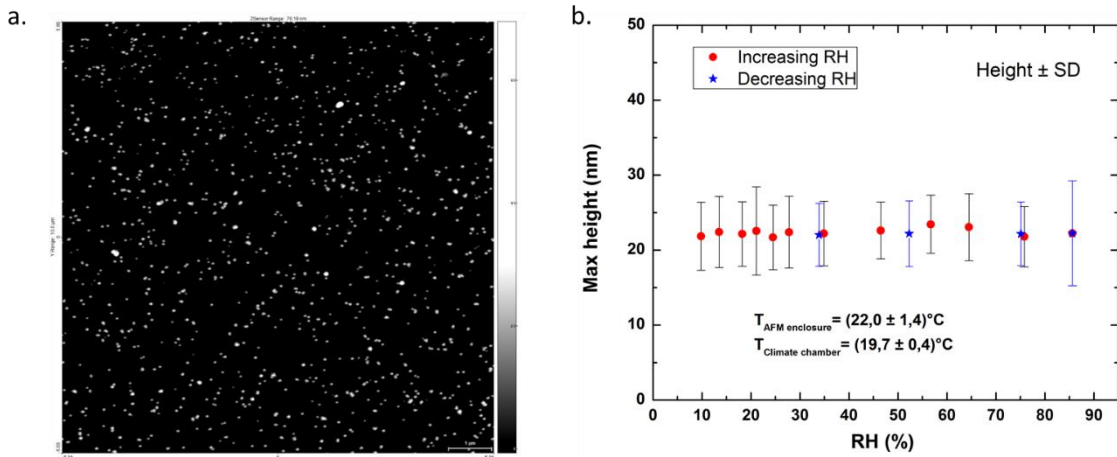


Figure 28. An example of a 10 × 10 μm² AFM image of the topography of the IRMM silica nanoparticles (a). Measured mean diameter of the nanoparticles for different humidity levels (b).

The experiment was repeated on the silica nanoparticle sample. The relative humidity was first increased from 11 % up to 86 % while keeping the temperature constant. The nanoparticles were characterized measuring the maximum height of isolated particles as the diameter of the nanoparticles. The results obtained are presented on Figure 28 b. The diameter of the nanoparticles is  $22.4 \pm 4.7$  nm at 13.5 % of relative humidity and did not vary with the humidity level.

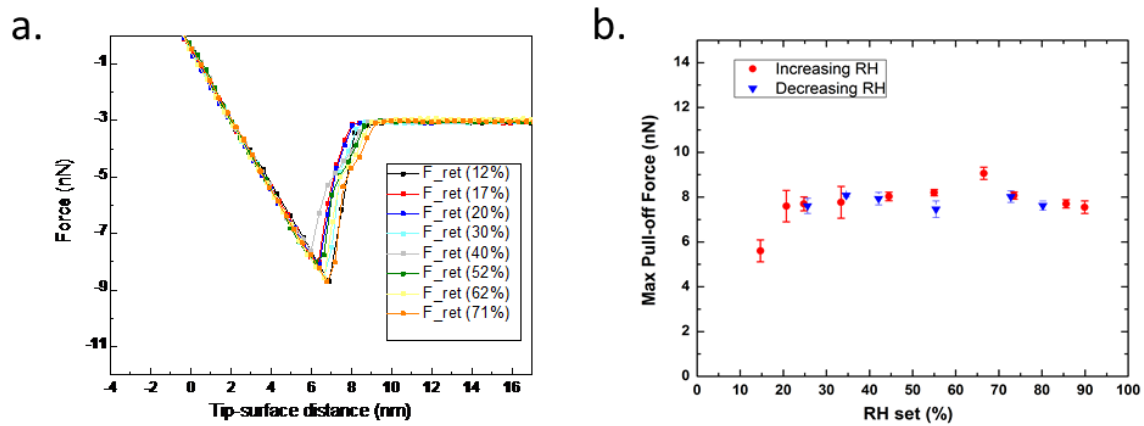


Figure 29. Examples of force-distance curves measured at different relative humidity level in the AFM enclosure (a). The represented curves were recorded during the retraction of the probe from the sample. Mean maximum pull-off force of the probe tip from mica substrate for different relative humidity (b). The data are represented as mean value ± standard deviation.

A series of Force-Distance experiment were also performed on a freshly cleaved mica substrates. The approach-retract curves were performed at a speed of 1 μm/s with a dwelling time of 1 s on the substrate before retraction of the probe. The F-D curves were continuously performed while varying the environmental conditions. The spring constant of the AFM cantilever was determined via the thermal tune method. A series of representative Force-distance curves (retraction part only) are presented on Figure 29 a. The maximum pull-off force was recorded while increasing and decreasing the relative humidity and keeping the temperature constant (Figure 29 b). The pull-off force measurements were recorded as the maximum adhesive force observed in the force-displacement curves during retraction. The reported pull-off force values are the averaging of at least 5 F-D curves. The maximum pull-off force slightly increase from  $5.6 \pm 0.5$  nN to  $7.6 \pm 0.7$  nN when increasing the relative humidity from 14.7 % to 20.7 %, respectively. The measured values are almost constant and not affected by variation of the relative humidity.

An increase in the humidity level can be related to an increase in the force required to pull-off the tip from the sample surface. This can be explained by a thicker water layer on the sample surface. However, this does not affect the sample height measurement.

### 4.3.3 Summary of key research outputs and conclusions

The project developed reference probes and samples to perform experiments for probe-sample elastic deformation analysis and performed various experiments and numerical studies related to the tip characterisation, tip elastic deformation and influence of humidity on AFM measurements were performed.

Experiments were performed on stepheight standards and nanoparticles samples using usual AFM probes with two different experimental set-ups to study the effect of the environmental conditions on the probe sample interaction during AFM measurement. The relative humidity was varied in a broad range from 10 % to 90 % and the temperature in a reduced range from 20 °C to 35 °C , these values cover the usual experimental conditions of AFM measurements. The studies on the effect of environmental conditions revealed that the effects from relative humidity and temperature are not significant within the experimental conditions covered in this study. These experimental conditions include the temperature and relative humidity but also the nature of the samples, the imaging conditions (imaging mode, scan speed) and the AFM cantilever (spring constant).

If novel types of high-aspect ratio SPM tips are being used for dimensional measurements, it is important to consider the potential elastic deformation of the tip, which could easily occur for higher forces. This is most likely the case of both repulsive forces used in contact mode, but for very thin tips can be also case of the combination of attractive and repulsive forces in the Tapping mode or similar dynamic regimes. By using the numerical and experimental tools developed in this project, one can estimate this contribution and use it in uncertainty analysis and in principle for systematic errors compensation.

From these investigations, it can be deduced that the tapping mode is much safer regime for measurements, especially with high aspect ratio probes, where the tendency for elastic deformation is much higher. This is fortunately the most widely used approach. The uncertainty related to measurement regime settings is then below one nanometre, and if the experimental conditions are kept unchanged even smaller can be reached.

## 4.4 Development of a hybrid metrology for merging measurement results

It is well recognised that the combination of multiple metrology techniques into “hybrid metrology” is a promising methodology to meet current measurement challenges. Data fusion combines measurement data from different instruments to improve the measurement accuracy by sharing extra information and rectifying inter-variable correlations. However, neither practical application with hybrid metrology nor software for data fusion were available prior to the start of the project. Although some solutions to combine data measured with different instruments did exist, these methods suffer from limitations in exchangeability of the information due to metrological limitations, e.g. lack of traceability and improper understanding of probe-sample interactions. Therefore, the project developed a metrological basis that allows for easily combining information between instruments for data fusion.

### 4.4.1 Software for data fusion

The simplest approach is to use multiple SPM measurements in order to reduce some potential scanning artefacts, like the data anisotropy related to presence of fast and slow scanning axis in SPM. This effect leads to errors during some sensitive data processing steps, like blind tip estimation. The simple methods like the direction change based data denoising [Ref. C2] were tested on project samples, as shown in Figure 30.

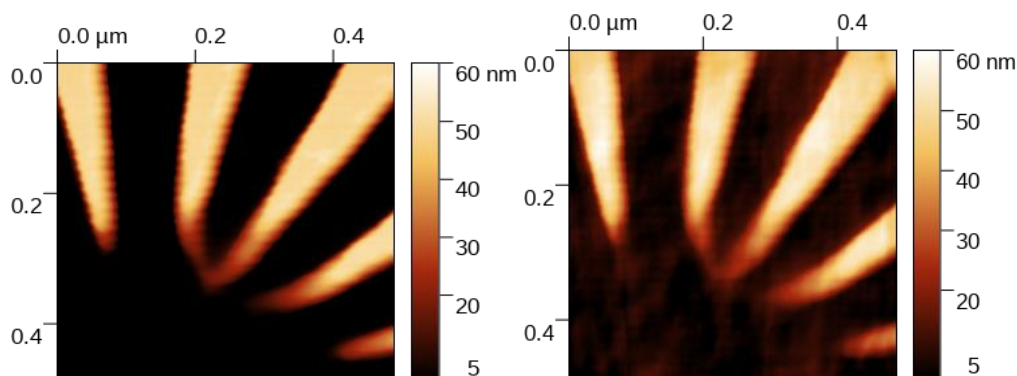


Figure 30. Reduction of the horizontal strike artefacts via xy denoising procedure, a detail on Siemens star sample is shown, (left) horizontal scan and (right) merged horizontal and vertical scan.

The more complex data processing, but still using only multiple SPM data was based on using different sample orientations plus different scan directions. For data fusion Gwyddion open source software was used, scripted via the PyGwy interface. In this way, use up to 24 different channels for a single data fusion was demonstrated on nanoindenter tips (12 topography and 12 adhesion channels). Nanoindentation measurements are very sensitive to the area function measurements, which can be done via SPM techniques. However, the scan defects can significantly reduce the reliability of such analysis. Using the multiple channel data fusion can lead to a better representation of the tip shape and the area function. An example of an individual topography and adhesion measurement is shown in Figure 31. An indenter area function from the merged dataset is shown in Figure 32.

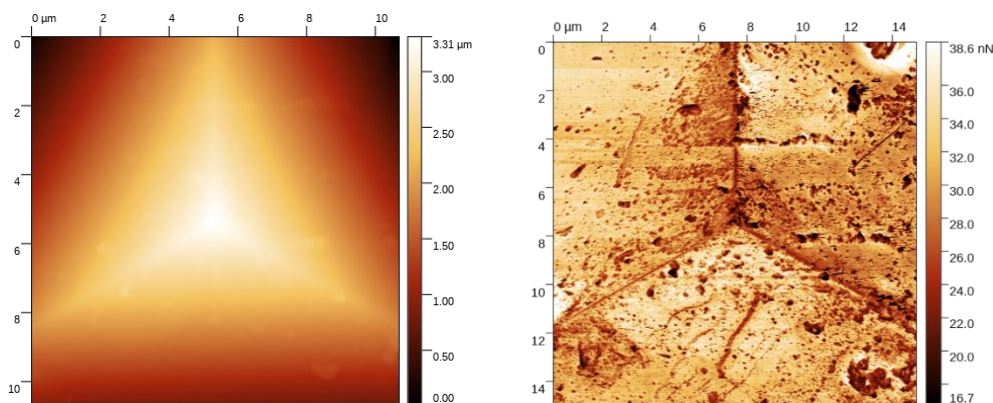


Figure 31. Typical nanoindenter tip topography (left) and adhesion channel (right).

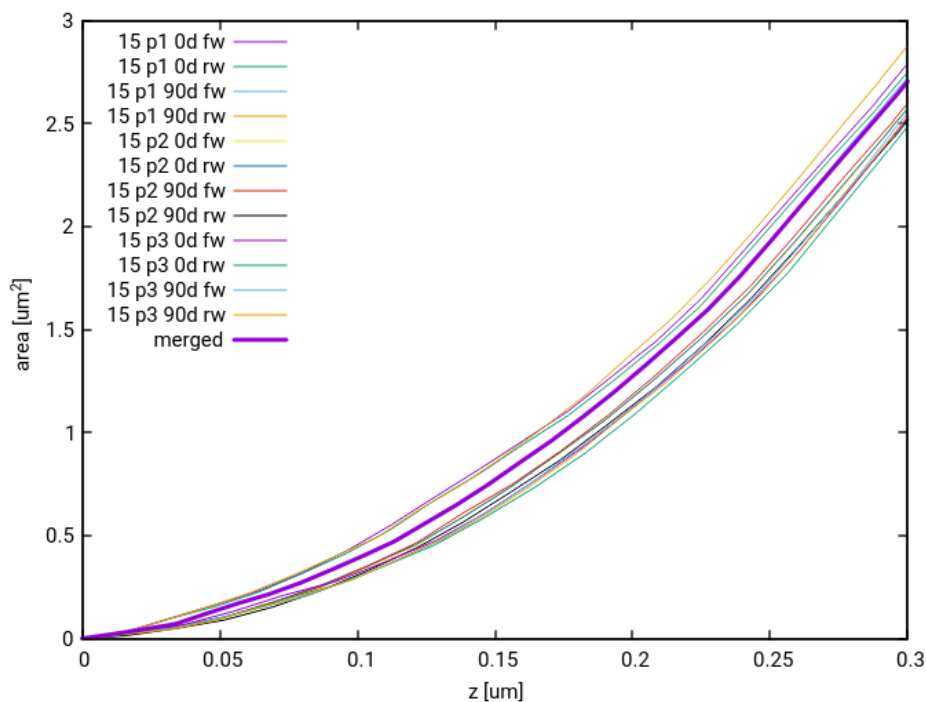


Figure 32. Resulting area functions from individual tip measurements (3 rotations, 2 scan orientations, 2 scan directions) and from the merged tip shape.

To analyze the different data fusion mechanisms we have also added simulation tools for the Siemens star samples to Gwyddion open source software as shown in Figure 33. These were used for the hybrid metrology methods development at CMI and are publicly available for future use.

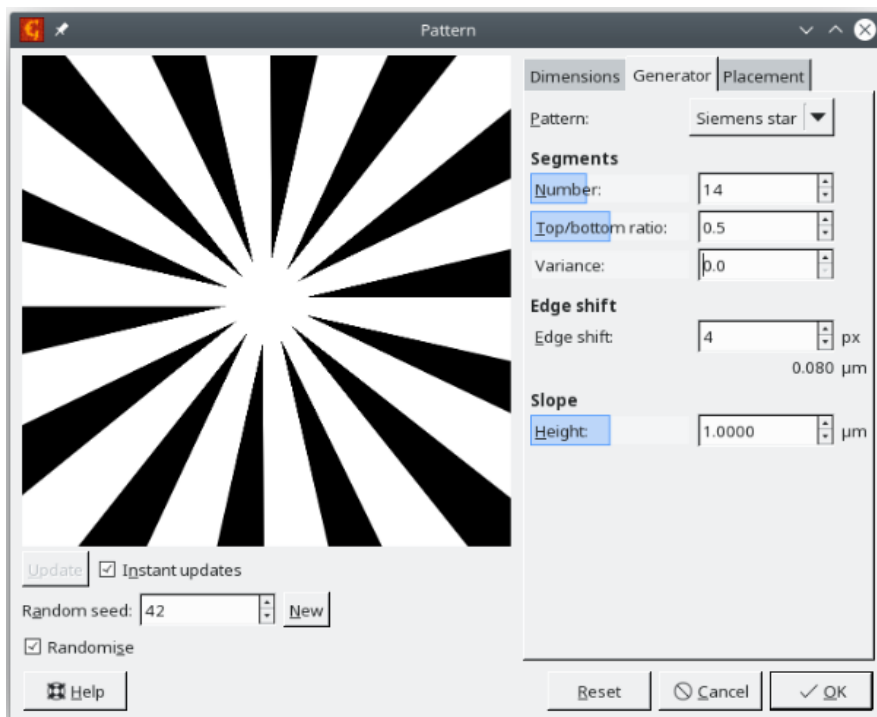


Figure 33. Gwyddion interface for a Siemens star sample surface.

#### 4.4.2 Hybrid metrology of AFM and TEM for bottom-up approach

All fusion methods for spatial data need a registration process to linearly transform different datasets to the same coordinate system before fusion. The accuracy of the data registration is a key factor impacting the performance of hybrid metrology. PTB introduced two methods applied for matching the measurement data of the TEM and AFM in the hybrid approach for realising the bottom-up approach see section 4.1.1.

The TEM results measured on the target structure needs to be transferred to that of the AFM results previously measured. It is required that the AFM and TEM results are from the same location. Unfortunately, the measurement conditions of the AFM and TEM are quite different. In AFM an area with a size of  $2.5\ \mu\text{m} \times 1.0\ \mu\text{m}$  is measured with typically 32 profiles, which delivers 32 groups of CD values; while the TEM measurement offers only one group of CD value from the TEM lamella, which is approximately 50 nm thick. The matching of the AFM and TEM results becomes a critical issue, since the mismatch will lead to significant measurement error due to the line width variation of the line features.

Two methods were applied to ensure the matching of the AFM and TEM measurements. One method uses alignment marks “written” near to the target feature pattern by the focus ion beam (FIB) milling. The other method uses the least square fitting of the AFM and TEM results.

By applying the hybrid method for determination of critical dimension a combined standard measurement uncertainty of the reference CD value is estimated as 0.81 nm. Five independent investigations were carried out to determine the CD of the same reference structure. The obtained CD values agree well with each other within the given uncertainty level.

#### 4.4.3 Hybrid metrology with optical scatterometry and MAFM

DFM combined optical methods including Mueller Polarimetry and scatterometry, which are fast and in-line measurement feasible but strongly model dependent, with AFM, which is capable of 3D measurement with high spatial resolution and precision but slow. The hybrid metrology approach was applied for characterising reference materials, especially the Siemens star and nanopillar samples. The results are shown in subsection 4.2.2 under the title "Hybrid metrology results".

#### 4.4.4 Summary of key research outputs and conclusions

Hybrid metrology methods for merging measurement results either from different channels of a single tool or different tools were developed. Fusion of datasets from multiple SPM measurements of the sample was used to reduce the scan artefacts like feedback loop defects and data anisotropy. For this data fusion, scripting available in Gwyddion open source software was used and combined with other data fusion modules. To test the reliability of this data fusion approach a set of simulated tip check samples was used together with different SPM artefacts simulation tools. Moreover, the impact of the potential probe-sample elastic deformation on such experiments was estimated; however, for most of the dimensional measurements using standard probes this effect was lower than the scan imperfections effect.

Two methods were developed for matching the measurement data of the TEM and AFM in the hybrid approach for realising the bottom-up approach. One method uses alignment marks “written” near to the target feature pattern by the focus ion beam (FIB) milling. The other method uses the least square fitting of the AFM and TEM results. By applying the hybrid approach for determination of critical dimension a combined standard measurement uncertainty of the reference CD value was estimated as 0.81 nm.

Optical methods including Mueller Polarimetry and scatterometry, which are fast and in-line measurement feasible but strongly model dependent, were combined with AFM, which is capable of 3D measurement with high spatial resolution and precision but slow. This hybrid metrology approach was applied for characterising reference materials, especially the Siemens star and nanopillar samples.

## 5 Impact

The project results were disseminated mainly by direct contact with industrial stakeholders. Nevertheless, ten open access peer-reviewed papers were published, and the project and its results were presented at various conferences (37 presentations in 21 conferences). Several presentations covering the developed methods, equipment as well as reference materials and artefacts were presented. Moreover, a Good Practice titled "Guide for dimensional metrology at the nanometre scale and for using the developed reference standards and methodologies" was developed and is available for download on the project website. The project results were presented also in two webinars. A software module for data fusion purposes was developed for Gwyddion, which is a free modular program for SPM data visualisation and analysis (<http://gwyddion.net>). This project delivered new and improved methods and reference materials for 3D measurements of nanostructures. Many of the methods and reference standards were developed in close co-operation with industry and several companies have already shown interest to exploit the project outcomes. The research outputs of the project allow traceable 3D metrology at the nanometre level with measurement uncertainties below 1 nm, which meet the requirements of industry or scientific research. By bringing traceability to the SI metre for 3D nano measurements, finally enables NMI to offer the long-awaited metrological support to industry. To assist the industrial and scientific communities, new SI traceable measurement and calibration services for CD measurements were launched.

### *Impact on industrial and other user communities*

This project improved dimensional nanometrology at nanometre scale in order to advance the development and expansion of European high technology industries. To ensure the industrial impact, many of the methods and equipment developed in the project were characterised by measuring samples received from industrial stakeholders and the calibration standards produced in the project were designed in close cooperation with the stakeholders. The consortium performed reference metrology of industrial photomask standards, which confirms the feasibility of the bottom-up and top-down metrology methodology developed in this project. The successful photomask standard case shows high potential that the method will be taken-up by industry.

PTB initiated collaboration with a company to exploit the developed 3D nanometrology to investigate the new industrial CD standard. The measurements results are expected to improve the products of an industrial stakeholder. Moreover, PTB is collaborating with a world-leading equipment vendor to exploit the developed 3D nanometrology to measure three-dimensional parameters (including height, width, sidewall angle, sidewall profile etc.) of complex nanostructures. This challenging and important metrology task is required for realising e.g. the next generation lithography (NGL) technologies. VTT and PTB measured the 3D geometry of several

types of optical specimens (microlens array MLA concave 6  $\mu\text{m}$  lens and MLA convex 1.5  $\mu\text{m}$  and 6  $\mu\text{m}$  lenses) received from industrial stakeholders. This collaboration demonstrated the measurement capabilities of the developed equipment and methods for industry.

INRIM collaborated with a parent institute (CNR-IPSP Institute for Sustainable Plant Protection) for developing the preparation of samples with known plant nanostructures. DFM developed a compact scatterometry setup and delivered it to the NIL technology ApS for field measurements on nanostructured surfaces. CMI further developed a software module for Gwyddion for data fusion purposes. The software is free and available at <http://gwyddion.net/>. Thousands of new downloads during the project period indicates its great impact for public communities. NPL developed EBD AFM tips that have been trialed by a UK AFM manufacturer supplying AFM systems for the semiconductor industry. VSL has received interest from two companies regarding the developed Siemens star samples. TNO was made aware of this and contact details have been exchanged.

#### *Impact on the metrology and scientific communities*

The key impact from this project to the metrological and scientific communities is the traceability of 3D nano measurements to the SI metre, which enables NMIs to offer metrological support to industry. When the project started, the traceability chain was broken, because the uncertainty levels of traceable measurements at NMIs did not meet the requirements of the scientific community and industry.

Results from the bottom up approach and the x-ray interferometry work performed within this project contributed to the realisation of the lattice parameter of silicon as a secondary length standard in the revised *Mise en Pratique* for the metre (<https://www.bipm.org/utis/en/pdf/si-mep/SI-App2-metre.pdf>) and to its Guidance document *CCL-GD-MeP-1*: "Realisation of the SI metre using silicon lattice parameter and x-ray interferometry for nanometre and sub-nanometre scale applications in dimensional nanometrology" (<https://www.bipm.org/utis/common/pdf/CC/CCL/CCL-GD-MeP-1.pdf>).

Two universities and a research institute were actively involved in the project as collaborators: University of Helsinki, Technische Universität Ilmenau and Institute for Sustainable Plant Protection. University of Helsinki provided nanostar samples that the partners used for measurements with different methods. The results of these measurements are described in a co-authored peer-reviewed paper titled "Transfer standards for 3D nano-metrology" (submitted). The University of Technology Ilmenau, verified with a frequency comb and a GPS system all three frequency-stabilised lasers (axes x, y, z of the FAU nanopositioning and manomeasuring machine). Institute for Sustainable Plant Protection (IPSP) supplied freshly grown bio-plant nanostructures, namely Tobacco Mosaic Virus (TMV). TMV has a rod shape with a diameter of about 18 nm, which represents a natural reference as tip characteriser for metrological Atomic Force Microscopes.

#### *Impact on relevant standards*

The consortium had active communication on EURAMET Technical Committee in Length (TC-L), Consultative Committee in Length (CCL) and CCL Working Group Nano (WG-N) on the new *Mise en Pratique* for realisation of the metre on nanometre scale. The project contributed to the realisation of the lattice parameter of silicon as a secondary length standard in the revised *Mise en Pratique* for the metre. Moreover, the project results were presented in a CCL WG-N meeting.

Documentary standard ISO 11952: – "Scanning-probe microscopy – Determination of geometric quantities using SPM: Calibration of measuring systems for the dimensional calibration of SPM instruments" was revised under PTB lead. In addition, the project had contacts with an Italian standardisation body (UNI/CT 047) and the following national standardisation committees UNI, METSTA, VDI/VDE and Dutch normcommission Nanotechnologie were informed about the project results. Results

#### *Longer-term economic, social and environmental impacts*

Advanced dimensional nanometrology is an enabling technology for the manufacture of nanotechnologies and research and therefore needed for re-industrialisation of Europe and for creating European wealth. Nanotechnologies and advanced materials have potential to offer valuable solutions in the health, energy, climate and environmental sectors, leading to economic growth in Europe.

The advanced nanometrology methods and reference materials developed in this project will benefit nanotechnology industries. The project established appropriate and urgently needed nanometrology capabilities and traceability for various nanoscale measurements, which provides competitive advantages for

European companies and supports future innovation. Furthermore, in long term the results will enhance the growth of nanotechnology industries e.g. the semiconductor, nanomaterial, nanophotonics, microscopy, etc.

Concerning energy, an improved nanomanufacturing industry will result in products with lower energy consumption, and it could lead to better energy harvesting capability. For example, the use of nanotechnology, more specifically organic photovoltaic cells instead of silicon crystal solar cells is making solar power cheaper. The developed 3D nanometrology methods can help to control nanoscale morphology, which could significantly increase the conversion efficiency of photovoltaic cells.

Clinical tests for nanomedicine and nanotoxicology lack comparability of data. Much progress has been made in labs around the world, but *because the measurement results have not been traceable*, they cannot be compared and few valuable conclusions can be drawn. The traceable methods developed in this project may help this. Furthermore, before any nanomedicine product is investigated in clinical tests, reliable measurement datasets are required, for which traceability is crucial.

## 6 List of publications

1. Petr Klapetek, Anna Charvátová Campbell, and Vilma Buršíková, "Fast mechanical model for probe-sample elastic deformation estimation in scanning probe microscopy", *Ultramicroscopy* **201**, 18–27 (2019). Available online: <https://doi.org/10.1016/j.ultramic.2019.03.010>.
2. Timo Strahlendorff, Gaoliang Dai, Detlef Bergmann, Rainer Tutsch, "Tip wear and tip breakage in high-speed atomic force microscopes", *Ultramicroscopy* **201**, 28–37 (2019), available online: <https://doi.org/10.1016/j.ultramic.2019.03.013>
3. Andrew Yacoot, Petr Klapetek, Miroslav Valtr, Petr Grolich, Herve Dongmo, Giovanni Mattia Lazzerini, and Angus Bridges, "Design and performance of a test rig for evaluation of nanopositioning stages", *Meas. Sci Technol.* **30**, 035002 (2019), available online: <https://doi.org/10.1088/1361-6501/aafd03>.
4. Johan Nysten, "A characterization and Monte Carlo evaluation of positioning uncertainty estimates of an MAFM", Master thesis, available online: <https://jyx.jyu.fi/handle/123456789/62847?locale-attribute=en>.
5. Janik Schaude, Julius Albrecht, Ute Klöpzig, Andreas C. Gröschl and Tino Hausotte, "Atomic force microscope with an adjustable probe direction and piezoresistive cantilevers operated in tapping-mode / Im Tapping-Modus betriebenes Rasterkraftmikroskop mit einstellbarer Antastrichtung und piezoresistiven Cantilevern", *tm – Technisches Messen* **86**, 12–16 (2019), available online: <https://doi.org/10.1515/teme-2019-0035>.
6. V. Constantoudis, G. Papavieros, P. Karakolis, A. Khiat, T. Prodromakis and P. Dimitrakis, "Impact of Line Edge Roughness on ReRAM uniformity and scaling", *Materials* **12**, 3972 (2019), <https://doi.org/10.3390/ma12233972>
7. Gaoliang Dai, Linyan Xu, Kai Hahm, "Sub-nm accurate tip characterization in critical dimension atomic force microscopy", accepted to *Meas. Sci. Technol.* Available online: <https://iopscience.iop.org/article/10.1088/1361-6501/ab7fd2>
8. E. Heaps, A. Yacoot, H. Dongmo, L Picco, O.D. Payton, F. Russell-Pavier, P. Klapetek, "Bringing real-time traceability to high-speed atomic force microscopy", accepted to *Meas. Sci. Technol.* Available online: <https://doi.org/10.1088/1361-6501/ab7ca9>
9. P. Klapetek, A. Yacoot, V. Hortvik, V. Duchon, H. Dongmo, S. Rerucha, M. Valtr, "Multiple fiber interferometry setup for probe sample interaction measurements in Scanning Probe Microscopy," DOI: 10.1088/1361-6501/ab85d8, available online: <https://iopscience.iop.org/article/10.1088/1361-6501/ab85d8>
10. V. Heikkinen, I. Kassamakov, T. Viitala, M. Järvinen, T. Vainikka, A. Nolvi, C. Bermúdez, R. Artigas, P. Martinez, V. Korpelainen, A. Lassila, and E. Hæggröm, "Step height standards based on self-assembly for 3D metrology of biological samples," available online: <https://doi.org/10.1088/1361-6501/ab8c6a>

## 7 Contact details

For further information on the results of the 3DNano project please contact the coordinator: Virpi Korpelainen ([virpi.korpelainen@vtt.fi](mailto:virpi.korpelainen@vtt.fi)).